Faraday Patterns in a Stack of Driven Quasi-One-Dimensional Dipolar Bose-Einstein Condensates

A Thesis

submitted to
Indian Institute of Science Education and Research Pune
in partial fulfillment of the requirements for the
BS-MS Dual Degree Programme

by

Shreyas Nadiger

IISER PUNE

Indian Institute of Science Education and Research Pune
Dr. Homi Bhabha Road,
Pashan, Pune 411008, INDIA.

April, 2024

Supervisor: Prof. Rejish Nath

© Shreyas Nadiger 2024

All rights reserved

Certificate

This is to certify that this dissertation entitled Faraday Patterns in a Stack of Driven Quasi-One-Dimensional Dipolar Bose-Einstein Condensatestowards the partial fulfilment of the BS-MS dual degree programme at the Indian Institute of Science Education and Research, Pune represents study/work carried out by Shreyas Nadigerat Indian Institute of Science Education and Research under the supervision of Prof. Rejish Nath, Associate Professor, Department of Physics , during the academic year 2023-2024.

Prof. Rejish Nath

Committee:

Prof. Rejish Nath

Prof. M. S. Santhanam

This thesis is dedicated to my mother

Declaration

I hereby declare that the matter embodied in the report entitled Faraday Patterns in a Stack of Driven Quasi-One-Dimensional Dipolar Bose-Einstein Condensates are the results of the work carried out by me at the Department of Physics, Indian Institute of Science Education and Research, Pune, under the supervision of Prof. Rejish Nath and the same has not been submitted elsewhere for any other degree. Wherever others contribute, every effort is made to indicate this clearly, with due reference to the literature and acknowledgement of collaborative research and discussions.

Shreyas

Shreyas Nadiger

Acknowledgments

I have been blessed with the support of several individuals throughout my time at IISER Pune. First and foremost, I thank my supervisor, Dr Rejish Nath, for his immense patience and care throughout my stay in his group. I am grateful for the opportunity and your guidance through undergraduate research. Your work ethic is something I greatly admire and will always strive towards. This project would not have been possible, of course, without the help of my group members, Inderpreet, Ratheejit and Sandra. Thank you for the numerous discussions, regarding this project or others. I also thank my other group members, Ashutosh, Siddharth and Varna for the making the work environment welcoming and enjoyable. I also thank Prof. Santhanam for being the expert for this thesis and also his wonderfully conducted courses.

I am also grateful for my past project guide, Dr Apratim Chatterji. Your enthusiastic attitude is contagious and I admire your relaxed and open nature with your students. I thank Adrian, Debarshi, Shreerang and Vaibhav for the amazing discussions, both academic and informal. I also thank Dr Bijay, Dr Suneeta, Prof Bhas and Dr Sreejith for their wonderfully conducted courses that laid the foundation for many of the concepts used in the thesis.

I thank the Department of Science and Technology(DST) India for the Kishore Vaigyanik Protsahan Yojana scholarship which has supported me throughout my time at IISER Pune. I also thank the support and resources provided by PARAM Brahma Facility under the National Supercomputing Mission, Government of India.

I am indebted to my group of friends for putting up with me and providing a second home at IISER. While this list is certainly not exhaustive, thank you[1] Abhijith, Abhinav, Arjun, Atharva, Gautham, Prathith, Ronedy, Sanjay, Shridhar, Soham, Subramanya, Vaishak and

---

[1] It's in alphabetical order, relax.

others I might have missed. I'm also thankful to Gautam, Prabhav and Purva for being incredibly helpful seniors.

Last but not least, I am incredibly fortunate and grateful to my family. Thank you Amma for always believing in me even when I couldn't and for your constant support and guidance. Thanks to my sister for always keeping the home environment lively and thanks to my grandmother for your care. Thank you appa for teaching me so much about everything.

Abstract

In this thesis, we study pattern formation in a stack of periodically driven quasi one-dimensional dipolar Bose-Einstein condensates. We study the excitation spectrum of the spatially separated dipolar condensates using Bogoliubov theory. The excitations are collective in nature due to the long-range nature of the dipole-dipole interaction. The parametric modulation of the s-wave scattering length leads to density modulations whose dynamics depends on the lowest Bogoliubov mode. The nature of the Bogoliubov modes depends on the orientation of the dipoles. When the dipoles are aligned such that the inter-tube dipolar interactions are attractive, the lowest mode corresponds to in-phase density modulations, leading to transient stripe patterns. In contrast, when the inter-tube interactions are repulsive, the lowest mode has out-of-phase character, resulting in checkerboard patterns. We also study the dynamics of quenching the dipole angle up on initial pattern formation and observe that it leads to a dynamical transition between the patterns.

Contents

Abstract **xi**

1 Introduction **3**

2 Faraday patterns in Bose-Einstein condensates **7**

2.1 Bose-Einstein condensation 7

2.1.1 Short-range interactions 8

2.1.2 The dipole-dipole interaction 10

2.1.3 Mean field description 12

2.1.4 Lower dimensional condensates 15

2.1.5 Elementary excitations 17

2.2 Faraday patterns 20

3 Setup and Bogoliubov excitations **25**

3.1 Setup 25

3.2 Bogoliubov spectrum 27

4 Stripe and checkerboard patterns **33**

4.1 Parametric driving 33

4.1.1 Stripe pattern 36

4.1.2 Checkerboard pattern 38

4.2 Abrupt quench 40

4.2.1 Stripe to checkerboard transition 40

4.2.2 Checkerboard to stripe transition 43

4.3 Linear quench 44

5 Summary and outlook **49**

A Mathieu equations **51**

References **55**

List of publications

- S Nadiger, SM. Jose, R Ghosh, I Kaur, and R Nath. “Stripe and checkerboard patterns in a stack of driven quasi-one-dimensional dipolar condensates”. In: *Phys. Rev. A* 109 (3 2024), p. 033309. DOI: 10.1103/PhysRevA.109.033309

Chapter 1

Introduction

The phenomenon of pattern formation has been widely studied in both classical and quantum systems. The analysis of the patterns and their underlying origin gives us valuable information about the instabilities of the system under study. Faraday patterns are a prominent example of pattern formation in periodically driven systems [1]. In Bose-Einstein condensates(BECs), periodic driving has been explored both theoretically [2–5] and experimentally [6–10] via parametric modulation of the s-wave scattering length or the periodic modulation of the optical lattice.

The dipole-dipole interactions(DDIs) are long-ranged and anisotropic in nature which gives rise to a range of interesting phenomena in quantum gases [11–15]. In contact-interacting BECs, physically separated condensates have no effect on each other and they can be treated as distinct systems. On the other hand, the long-range nature of the DDIs leads to interlayer effects which can have consequences on the collective phenomena and stability [11, 16–21]. Additionally, they also lead to hybrid excitations [22–24], soliton complexes [20, 25] and coupled density patterns [26]. Recently, an experiment on a stack of bilayers of dipolar ^{162}Dy($\mu = 10\mu_B$ where μ_B is the Bohr magneton) atoms observed strong dipole-dipole interactions via inter-layer cooling and coupled collective excitations [27]. This was possible due to a new super-resolution scheme that allowed them to reduce the spacing between two layers from the previous standard of 500nm to 50nm which means that the dipolar effects are 1000 times stronger. Additionally, the long-sought condensation of dipolar molecules was achieved [28, 29] through improved collisional shielding techniques to reduce the two and three body losses. These developments open up several prospects of novel physics, including inter-layer effects, dipolar droplets, self-organized crystal phases and dipolar spin liquids in optical lattices.

In this thesis, we study transient density patterns in a stack of quasi one-dimensional dipolar BECs via parametric modulation of the s-wave scattering length. The inter-tube DDIs lead to collective modes which are described by Bogoliubov theory. We therefore study the Bogoliubov spectrum for two different orientations of the dipoles. When the inter-tube interactions are attractive, the excitation of the lowest mode leads to a stripe density pattern, whereas repulsive inter-tube interactions lead to a checkerboard pattern. We shall also study the quenching of the dipolar angle, which leads to a dynamic transition between patterns.

The structure of the thesis is as follows:

- **Chapter 2:** We discuss the general phenomenon of Bose-Einstein condensation and the phenomenon of Faraday pattern formation. We first discuss the weakly-interacting BECs with short-range interactions and move on to discuss dipolar BEcs - their mean-field description, introduce the Gross-Pitaevskii equation(GPE) and also discuss condensates in lower dimensions and elementary excitations. We then introduce Faraday patterns and discuss Faraday patterns in nondipolar and dipolar BECs.

  Chapters 3 and 4 discuss the results obtained in [30].

- **Chapter 3:** This chapter introduces the model and discusses the Bogoliubov spectrum. We discuss the governing GPEs and the corresponding Bogoliubov-de Gennes equations for our setup. We obtain the Bogoliubov spectrum for two different dipolar orientations and show that the lowest mode in the Bogoliubov spectrum can be engineered to be in phase or out of phase density modulations depending on the dipole orientation.

- **Chapter 4:** In this chapter, we discuss the parametric driving of the s-wave scattering length which excites the lowest Bogoliubov mode and leads to transient stripe and checkerboard patterns. We then discuss the dynamics of quenching the dipole angle. We observe a dynamical transition between the patterns upon quenching the dipole angle once the initial pattern is formed. We study the abrupt and linear quench scenarios.

- **Chapter 5:** We provide the summary and outlook of the thesis.

Chapter 2

Faraday patterns in Bose-Einstein condensates

Ultracold atomic and molecular gases have attracted considerable attention since the experimental observation of Bose-Einstein condensation and quantum degenerate Fermi gases. Much of the interest in these systems is due to the incredible degree of control and tunability they offer. As such, these systems serve as a test bed for theoretical predictions from conventional condensed matter systems to even high-energy physics. Interparticle interactions are at the core of much of the properties of matter. Even in the weakly interacting regime, the shape, density and excitations are dictated by interactions. Below, we describe the general phenomenon of Bose-Einstein condensation, starting from the weakly interacting Bose gases with short-range interactions.

2.1 Bose-Einstein condensation

The phenomenon of Bose-Einstein condensation was first predicted by Einstein in 1924 [31] after S. N. Bose had proposed quantum statistics for quanta of light, now known as photons [32]. Einstein extended the ideas to massive particles and predicted that at extremely low temperatures, non-interacting bosons would condense into a single quantum state. In the grand-canonical ensemble, the occupation number of a quantum state with energy ϵ_i is given by

$$\langle n_i \rangle = f(\epsilon_i) = \frac{1}{e^{(\epsilon_i - \mu)/k_B T} - 1} \tag{2.1}$$

where T is the temperature and μ is the chemical potential - the change in the energy of the system upon the addition or removal of a particle. The above equation requires $\mu < \epsilon_0$ in order to be consistent where ϵ_0 is the ground state energy of the gas. However, the occupation of the ground state becomes macroscopic when $\mu \to \epsilon_0$. This is the phenomenon of Bose-Einstein condensation.

The discussion of the ideal Bose gas, although it is instructive, remains primarily academic. Inter-particle interactions dramatically alter the properties of Bose-Einstein condensates even when the gases are very dilute. The interactions are described by scattering theory, specifically the scattering length of the processes involved. These scattering processes are sufficiently described at low enough temperatures by the s-wave scattering length. In a sufficiently dilute gas, the mean separation between two particles is larger than the s-wave scattering length. Below, we discuss weakly interacting Bose gases, starting with a brief description of short-range interactions.

2.1.1 Short-range interactions

The energy is extensive in the thermodynamic limit for a system of particles with contact interactions. This means that the following integral for the interaction potential $U(\mathbf{r})$ converges at large distances

$$\int_{r_0}^{\infty} d^D r U(\mathbf{r}) \tag{2.2}$$

where D is the dimensionality and r_0 is some cut-off. For $U(\mathbf{r})$ that go as $1/r^n$, this means that $D < n$ for short-range interactions.

The actual interaction potential $U(r)$ is non-trivial to incorporate while solving for $\psi(r)$. Instead, we focus on the most relevant information provided by $U(r)$, the s-wave scattering length. We therefore replace the actual potential with one that reproduces the correct scattering length and is easier to perform calculations with. The simplest form of potential satisfying the above requirements is the zero-range potential

$$U(\mathbf{r} - \mathbf{r}') = g\delta(\mathbf{r} - \mathbf{r}') \tag{2.3}$$

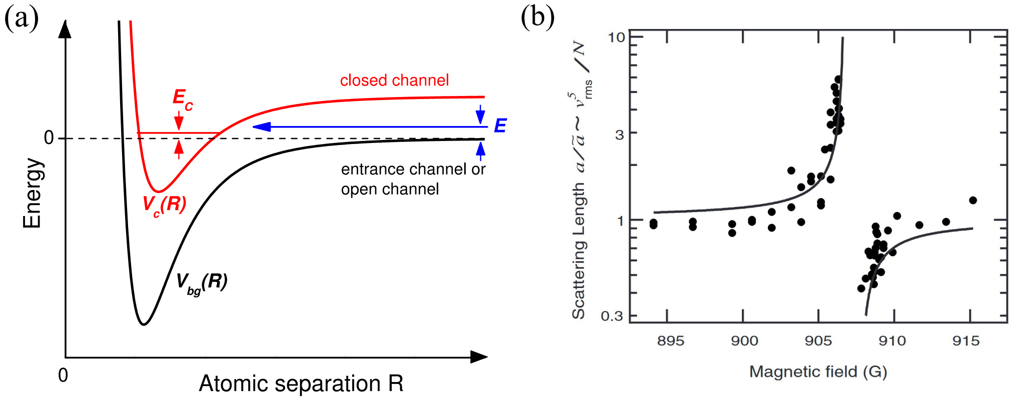

Figure 2.1: (a) A two channel model illustrating the coupling between the entrance(open) channel with energy E and the bound(closed) channel of energy E_c. The relative energy $E - E_c$ can be tuned via external magnetic fields. (b) Experimental observation of a magnetically tuned Feshbach resonance in a Bose-Einstein condensate of sodium atoms. The scattering length diverges near the resonance and leads to a loss of atoms from the trap. The figure is taken from [33].

which, using the Born approximation and the form of scattering amplitude in the low energy limit, gives the short-range coupling strength

$$g = \frac{4\pi\hbar^2 a_{sc}}{m} \tag{2.4}$$

In the above equations, we have ignored a regularization operator that becomes important if the wavefunction has a $1/r$ divergence but is irrelevant in the $r \to 0$ limit. Eq. 2.3 together with Eq. 2.4 will be used throughout our discussion to model the short-range interactions. We also note that $|ka_{sc}| \ll 1$ for the model potential to accurately describe the interactions in the system.

Tuning the short-range interactions

One of the main reasons for the interest in ultracold systems is their incredible degree of control and tunability. In addition to controlling the strength of inter-particle interactions ranging from strong to weak interactions, we can even alter the nature of these interactions from attractive to repulsive and vice versa. This can be done through magnetic or optical *Feshbach resonances*(FRs), where, in the presence of an external field, the scattering length undergoes large fluctuations.

A scattering or a collisional channel corresponds to a distinct scattering potential $V_{ch}(r)$. In Feshbach resonances, these distinct channels can be coupled by off-diagonal terms of the potential at finite r. Furthermore, the dissociation thresholds($V_{ch}(r \to \infty)$) can be tuned relative to one another(using magnetic fields in magnetic FRs for example). The two colliding atoms have kinetic energy E above the threshold E_{op} and are said to be in the open channel(the potential $V_{bg}(r)$ in Fig. 2.1), as they can be infinitely far away from each other. In contrast, a closed channel(the potential $V_c(r)$ in Fig. 2.1) has a higher dissociation energy $E_{cl} > E$. The off-diagonal terms induce the mixing of the two channels, and the atoms temporarily form a quasi-bound state which alters the scattering properties of the colliding pair, thereby changing the scattering length.

Particularly, when the corresponding magnetic moments are different, one can use magnetic fields to tune the relative energy of the channels, $E_{cl} - E_{op}$ in a magnetically tuned Feshbach resonance. The scattering length a can be tuned with the magnetic field B around the resonance B_0 as

$$a(B) = a_{bg}\left(1 - \frac{\Delta}{B - B_0}\right) \tag{2.5}$$

where a_{bg} is the background scattering length associated with the open channel($V_{bg}(r)$), and Δ is the resonance width which relates to the strength of the coupling between the bound and scattering states. Such magnetic FRs are routinely used in ultracold atom experiments, for a review, see [12] and [33]. Apart from magnetic FRs, optical Feshbach resonances have been proposed and demonstrated in alkali, alkaline earth and non-magnetic lanthanides [34–37]. They are useful as they allow ultrafast and local control of inter-particle interactions. However, optical Feshbach resonances have yet to be demonstrated in magnetic atoms but are promising in lanthanides due to their spectra.

2.1.2 The dipole-dipole interaction

In general, the interaction between two dipoles with dipole moment d(can be electric or magnetic moment) and position vectors $\mathbf{r}_1$ and $\mathbf{r}_2$ with the separation vector $\mathbf{r}$ is given by

$$V_d(\mathbf{r}) = g_d \frac{\hat{\mathbf{r}}_1 \cdot \hat{\mathbf{r}}_2 - 3(\hat{\mathbf{r}}_1 \cdot \hat{\mathbf{r}})(\hat{\mathbf{r}}_1 \cdot \hat{\mathbf{r}})}{r^3} \tag{2.6}$$

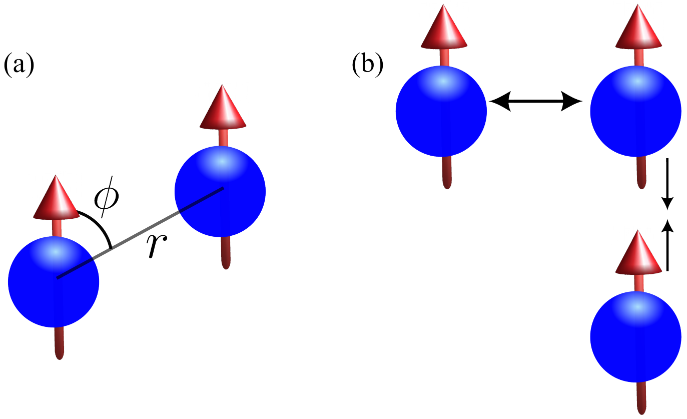

Figure 2.2: The long-range and anisotropic nature of the dipole-dipole interaction. (a) Two dipoles oriented in the same direction interact via the long range dipolar force. (b) Head-to-tail dipoles are attractive, whereas side-by-side dipoles repel each other.

where, in case of electric dipoles, $g_d = d^2/4\pi\epsilon_0(\epsilon_0$ is the vacuum permittivity) and for magnetic dipoles, $g_d = \mu_0 d^2/4\pi(\mu_0$ is the vacuum permeability). When the dipoles are polarized along the same direction(Fig. 2.2), we can simplify the expression to

$$V_d(\mathbf{r}) = g_d \frac{1 - 3\cos^2\theta}{r^3} \tag{2.7}$$

θ is the angle between the polarization direction and the separation vector. In section 2.1.1, we saw that the short-range interactions lead to extensive energy in the thermodynamic limit and $D < n$ for a short-range potential that goes as $1/r^n(D$ is the dimensionality). In contrast, dipolar interactions are long-ranged in 3D as they go as $1/r^3$. The anisotropy of the DDIs can be seen from Eq. 2.7 as θ varies from 0 to $\pi/2$, the factor $1-3\cos^2\theta$ varies from -2 to 1 which implies that for dipoles oriented head-to-tail($\theta = 0$) the DDI is attractive whereas for side-by-side dipoles($\theta = \pi/2$), the dipolar interactions are repulsive(see Fig. 2.2) and for $\theta = \arccos 1/\sqrt{3}$, the DDI are zero. The dipolar interactions also modify the scattering properties of the condensate. Due to their long-range nature, the phase shifts $\delta_l \sim k$ at low k for all partial waves, and hence, we need to consider the contributions from all partial waves.

2.1.3 Mean field description

The many-body Hamiltonian of N interacting bosons in an external trap V_{ext} is given by

$$\hat{H} = \int d\mathbf{r}\hat{\Psi}^{\dagger}(\mathbf{r})\left[\frac{-\hbar^2}{2m}\nabla^2 + V_{ext}(\mathbf{r})\right]\hat{\Psi}(\mathbf{r}) + \frac{1}{2}\int d\mathbf{r}\int d\mathbf{r}'\hat{\Psi}^{\dagger}(\mathbf{r})\hat{\Psi}^{\dagger}(\mathbf{r}')V(\mathbf{r}-\mathbf{r}')\hat{\Psi}(\mathbf{r}')\hat{\Psi}(\mathbf{r}) \tag{2.8}$$

where $\hat{\Psi}^{\dagger}(\mathbf{r})$ and $\hat{\Psi}(\mathbf{r})$ are the bosonic field operators that create and annihilate a particle at position $\mathbf{r}$ respectively and $V(\mathbf{r}-\mathbf{r}')$ is the inter-particle interaction potential. For short-range interacting gases, the inter-atomic potential is the delta potential discussed previously. In the presence of DDIs, $V(\mathbf{r}-\mathbf{r}')$ is modified to

$$V(\mathbf{r}-\mathbf{r}') = V_{sr}(\mathbf{r}-\mathbf{r}') + V_d(\mathbf{r}-\mathbf{r}') = g\delta(\mathbf{r}-\mathbf{r}') + g_d\frac{1-3\cos^2\theta}{|\mathbf{r}-\mathbf{r}'|^3} \tag{2.9}$$

which was first discussed by L. You and S. Yi [38, 39] for the general case of anisotropic potentials using the ladder approximation. The field operators obey the usual bosonic commutation relations:

$$[\hat{\Psi}(\mathbf{r}), \hat{\Psi}^{\dagger}(\mathbf{r}')] = \delta(\mathbf{r}-\mathbf{r}'), \qquad [\hat{\Psi}(\mathbf{r}), \hat{\Psi}(\mathbf{r}')] = 0, \qquad [\hat{\Psi}^{\dagger}(\mathbf{r}), \hat{\Psi}^{\dagger}(\mathbf{r}')] = 0 \tag{2.10}$$

However, it is often difficult to deal with the entire many-body Hamiltonian and hence it is converted to a single body problem through the mean-field approach. Instead of solving for all the pairwise interactions of a particle, we assume that the particle is in a potential that is averaged over all its interactions. The field operators are written in terms of single particle states $\phi_k(\mathbf{r})$ and the creation and annihilation operators as

$$\hat{\Psi}(\mathbf{r}) = \sum_k \phi_k(\mathbf{r})\hat{a}_k \qquad \text{and} \qquad \hat{\Psi}^{\dagger}(\mathbf{r}) = \sum_k \phi_k(\mathbf{r})\hat{a}_k^{\dagger} \tag{2.11}$$

The field operator can be separated into the condensate($k=0$) term and the non-condensate terms($k \neq 0$)

$$\hat{\Psi}(\mathbf{r}) = \phi_0(\mathbf{r})\hat{a}_0 + \sum_{k\neq 0}\phi_k(\mathbf{r})\hat{a}_k \tag{2.12}$$

In the limit of macroscopic occupation of the condensate state, $N_0 \simeq N$, the operators $\hat{a}_0$ and $\hat{a}_0^{\dagger}$ can be approximated by the c-number $\sqrt{N_0}$. This was first proposed by Bogoliubov in the context of superfluidity and is known as the Bogoliubov approximation [40]. This is equivalent to treating the condensate term as a classical field and Eq. 2.12 can be rewritten as

$$\hat{\Psi}(\mathbf{r}) = \psi_0(\mathbf{r}) + \delta\hat{\Psi}(\mathbf{r}) \tag{2.13}$$

The function $\psi_0(\mathbf{r})$ is the expectation of the field operator and is treated as the wave function of the condensate, $\psi_0(\mathbf{r}) = \langle\hat{\Psi}(\mathbf{r})\rangle = |\psi_0(\mathbf{r})|e^{iS_0(\mathbf{r})}$ where $S_0(\mathbf{r})$ is the phase of the condensate and is related to the coherence. The order parameter is non-zero in the condensate phase and vanishes in the non-condensed phase. We can also see that the $U(1)$ symmetry(here, the ability to choose the phase without affecting physical properties) is spontaneously broken in the condensate phase as it chooses a particular phase and hence, serves to characterize the phase transition. The Off-Diagonal Long Range order(ODLRO) of the BEC state can be described by $\psi_0(\mathbf{r})$. The one-body density matrix is given by

$$\rho(\mathbf{r} - \mathbf{r}') = \langle\hat{\Psi}^\dagger(\mathbf{r})\hat{\Psi}(\mathbf{r}')\rangle \tag{2.14}$$

A system is said to possess ODLRO if in the limit $\mathbf{r} - \mathbf{r}' \to 0$, the density matrix is non-zero, $\rho(\mathbf{r} - \mathbf{r}') \neq 0$.

$$\lim_{\mathbf{r}-\mathbf{r}'\to 0} \rho(\mathbf{r} - \mathbf{r}') \approx \langle\hat{\Psi}^\dagger(\mathbf{r})\rangle \langle\hat{\Psi}(\mathbf{r})\rangle = \psi^*(\mathbf{r})\psi(\mathbf{r}) = n_0 \tag{2.15}$$

where n_0 is the density of the BEC.

Gross-Pitaevskii equation

The time evolution of the field operator in the Heisenberg picture is given as

$$\begin{aligned} i\hbar\frac{\partial}{\partial t}\hat{\Psi}(\mathbf{r}, t) = [\hat{\Psi}(\mathbf{r}, t), \hat{H}] = \Bigg[&\frac{-\hbar^2}{2m}\nabla^2 + V_{ext}(\mathbf{r}, t) \\ &+ \int d\mathbf{r}'\hat{\Psi}^\dagger(\mathbf{r}', t)V(\mathbf{r} - \mathbf{r}')\hat{\Psi}(\mathbf{r}', t)\Bigg]\hat{\Psi}(\mathbf{r}, t) \end{aligned} \tag{2.16}$$

At zero temperature, all the particles are in the condensate and we can ignore the non-condensate part in Eq. 2.13 and replace the field operator by its expectation, the condensate wave function $\psi_0(r)$. We also employ the two-body potential(Eq. 2.9) to arrive at the

Gross-Pitaevskii equation(GPE) for the dynamics of the condensate

$$i\hbar\partial_t\psi(\mathbf{r},t) = \Bigg[-\frac{\hbar^2}{2m}\nabla^2 + V_{ext}(\mathbf{r}) + g|\psi(\mathbf{r},t)|^2 \\ + \int d\mathbf{r}'|\psi(\mathbf{r}',t)|^2 V_d(\mathbf{r}-\mathbf{r}')\Bigg]\psi(\mathbf{r},t) \tag{2.17}$$

which is an integro-differential equation. Eq. 2.17 is also known as Non-linear Schrödinger equation and was independently derived by Eugene Gross and Lev Pitaevskii [41, 42].

The time-independent GPE describes the steady state of a Bose-Einstein condensate near zero temperature. It can be derived from the many-body Hamiltonian(see Eq. 2.8) assuming a Hartree-Fock ansatz for the condensate wave function and we obtain the following equation for the energy functional[1]

$$E[\psi] = \int d\mathbf{r}\Bigg(-\frac{\hbar^2}{2m}|\nabla\psi|^2 + V_{ext}|\psi|^2 + \frac{g}{2}|\psi|^4 \\ + \frac{1}{2}|\psi|^2\int d\mathbf{r}'|\psi(\mathbf{r}')|^2 V_d(\mathbf{r}-\mathbf{r}')\Bigg) \tag{2.18}$$

which can be minimised to obtain the ground state of the dipolar BEC(dBEC) [11, 14, 43]. The validity of the above mean-field description has been explored in Refs. [44, 45] using the diffusive Monte Carlo(DMC) method. The conclusion was that the GPE remains valid away from shape resonances and as long as the effect of dipolar interactions on the s-wave scattering length is taken into account. Although we have ignored the effect of DDIs on the coupling parameter g, it is still valid as the main contribution to the dipolar integral in Eq. 2.17 comes from large inter-particle distances [13]. The above equation is then variationally solved to obtain the time-independent GPE

$$\mu\psi(\mathbf{r}) = \left(-\frac{\hbar^2}{2m}\nabla^2 + V_{ext} + g|\psi(\mathbf{r})|^2 + \int d\mathbf{r}'|\psi(\mathbf{r}')|^2 V_d(\mathbf{r}-\mathbf{r}')\right)\psi(\mathbf{r}) \tag{2.19}$$

Here, μ appears as a Lagrange multiplier, and physically represents the chemical potential of the system. It is now easy to see that the stationary solution of Eq. 2.19 is given by $\psi_0(\mathbf{r},t) = \psi_0(\mathbf{r})e^{-i\mu t/\hbar}$.

---

[1] We have assumed a time-independent potential for which the energy is conserved.

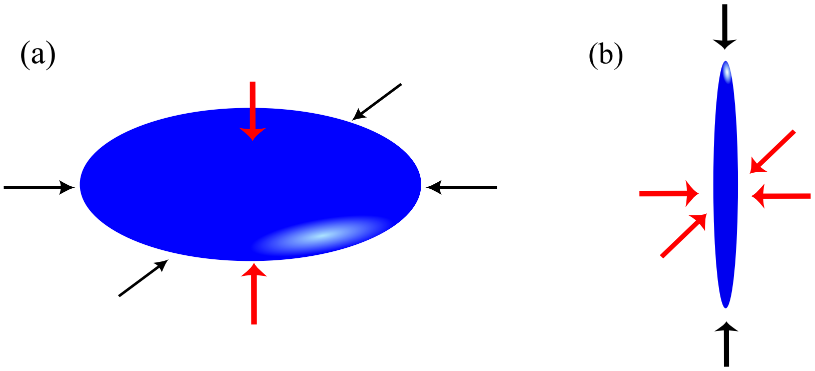

Figure 2.3: Lower dimensional condensates. (a) Quasi two-dimensional condensate. (b) Quasi one-dimensional condensate. Red and black arrows denote strong and weak confinement respectively.

2.1.4 Lower dimensional condensates

The properties of the condensate change drastically when the condensate is constrained along one or more directions. Such systems have been analyzed both theoretically [46–48] as well as experimentally [49–51] due to the advancements in trapping techniques.

In a 3D BEC, the relevant length scales are the radial extension of the BEC cloud R_ρ, its axial length R_z and its healing length ξ which is the minimum distance over which the condensate *heals* or in other words, returns to its bulk value when it is locally perturbed. It can be derived by equating the quantum pressure and the interaction terms $\hbar^2/m\xi^2 = gn$ giving $\xi = \hbar/\sqrt{mgn}$. When $R_\rho, R_z \gg \xi$, the condensate is in the three dimensional regime. However, under tight confinement in one or more directions, the condensate particles can only perform zero-point oscillations along the tightly confined directions and the dynamics is reduced to the weakly confined direction.

We consider the external potential to be harmonic, $V(x,y,z) = \frac{1}{2}m(\omega_\rho^2(x^2+y^2)+\omega_z^2 z^2)$(cylindrical symmetry) and the corresponding lengths $l_i = \sqrt{\hbar/m\omega_i}$. When $R_\rho \gg \xi \gg R_z$ or equivalently when $\hbar\omega_z \gg gn \gg \hbar\omega_\rho$, then condensate is said to be in the quasi 2-D regime and the condensate appears pancake shaped(Fig. 2.3). The condensate does not have sufficient energy to overcome the confinement along the strongly confined direction and hence, we can approximate the wave function along the strongly confined direction to be in the harmonic ground state $\phi(z) = \frac{1}{\pi^{1/4}\sqrt{l_z}} e^{-z^2/2l_z^2}$. We can separate the total wave function as

$\psi(x,y,z,t) = \psi(x,y,t)\phi(z)$ and then integrate over z in Eq. 2.17 to obtain the quasi 2-D GPE

$$i\hbar\frac{\partial}{\partial t}\psi(x,y,t) = \Bigg[-\frac{\hbar^2}{2m}(\partial_x^2 + \partial_y^2) + V_{ext}(x,y) + g_{2D}|\psi(x,y,t)|^2 \\ + \int dz|\phi(z)|^2 \int d\mathbf{r}'|\psi(\mathbf{r}',t)|^2 V_d(\mathbf{r}-\mathbf{r}')\Bigg]\psi(x,y,t) \quad (2.20)$$

where $g_{2D} = \frac{g}{\sqrt{2\pi}l_z}$ is the effective 2D coupling parameter.

A BEC is in the quasi 1D regime when $R_\rho \ll \xi \ll R_z$ or equivalently $\hbar\omega_\rho \gg gn \gg \hbar\omega_z$. As we did previously, we assume the radial wave functions to be in the harmonic ground state and separate the wave function into radial and axial parts,

$$\psi(x,y,z,t) = \phi_\rho(x,y)\psi(z,t) \quad (2.21)$$

where $\phi_\rho(x,y) = \frac{1}{\sqrt{\pi}l_\rho}e^{-(x^2+y^2)/2l_\rho^2}$. Again, integrating out the radial directions, we get the quasi 1D GPE

$$i\hbar\frac{\partial}{\partial t}\psi(z,t) = \Bigg[-\frac{\hbar^2}{2m}\partial_z^2 + V_{ext}(z) + g_{1D}|\psi(z,t)|^2 \\ + \int dxdy|\phi_\rho(x,y)|^2 \int d\mathbf{r}'|\psi(\mathbf{r}',t)|^2 V_d(\mathbf{r}-\mathbf{r}')\Bigg]\psi(z,t) \quad (2.22)$$

with $g_{1D} = \frac{g}{2\pi l_\rho^2}$. Physically, the condensate is an "oblate" form where it is elongated along z direction(Fig. 2.3). Such a condensate is also known as cigar-shaped due to its apparent resemblance. Quasi 1D geometry can also be used to study strongly correlated systems such as the Tonks-Girardeau gas, which can be described by the hard-core limit($g \to \infty$) of the Lieb-Liniger model [12, 52, 53]. This system has been used to study thermalization in 1D Bose gases and it was experimentally shown that the system is integrable and hence doesn't thermalize [54]. However, the addition of DDIs breaks the integrability [55].

2.1.5 Elementary excitations

In this section, we shall describe small deviations from the condensed phase, i.e. the changes in the condensate wave function are small with respect to the stationary solution. We consider small deviations of the condensate wave function from the mean-field solution of the form

$$\Psi(\mathbf{r},t) = \psi(\mathbf{r},t) + \delta\psi(\mathbf{r},t) = \psi(\mathbf{r},t) + u(\mathbf{r})e^{-i\omega t} + v^*(\mathbf{r})e^{i\omega t} \tag{2.23}$$

Substituting this ansatz(called the Bogoliubov ansatz) in the GPE and linearizing around the ground state wave function $\psi(\mathbf{r})$, we arrive at the coupled Bogoliubov de Gennes equations for a dipolar condensate

$$\begin{aligned} \left[-\frac{\hbar^2}{2m}\nabla^2 - \mu + V_{ext}(\mathbf{r}) + 2\Phi_{dd}(\mathbf{r}) \right] u(\mathbf{r}) + \Phi_{dd}(\mathbf{r})v(\mathbf{r}) &= \hbar\omega u(\mathbf{r}) \\ \left[-\frac{\hbar^2}{2m}\nabla^2 - \mu + V_{ext}(\mathbf{r}) + 2\Phi_{dd}(\mathbf{r}) \right] v(\mathbf{r}) + \Phi_{dd}(\mathbf{r})u(\mathbf{r}) &= -\hbar\omega v(\mathbf{r}) \end{aligned} \tag{2.24}$$

where we have introduced $\Phi_{dd}(\mathbf{r}) = \int d\mathbf{r}' V(\mathbf{r}-\mathbf{r}')|\psi(\mathbf{r}')|^2$ for clarity and $V(\mathbf{r})$ is the combined potential defined in Eq. 2.9. We can see that these equations are reduced to the non-dipolar case when we exclude the dipolar contributions. Generally, the BdG equations require numerical solutions for the energies and eigenfunctions. In special cases however, analytical solutions can be derived which provide us valuable insights. Consider a uniform(homogeneous) gas. Its ground state can be assumed to be constant $\psi_0(\mathbf{r}) = \sqrt{n}$ and the eigenfunctions of the excitations are simply plane waves,

$$u(\mathbf{r}) = \frac{1}{\sqrt{V}} u_q e^{i\mathbf{q}.\mathbf{r}}, \quad v(\mathbf{r}) = \frac{1}{\sqrt{V}} v_q e^{i\mathbf{q}.\mathbf{r}} \tag{2.25}$$

The excitation spectrum is the famous Bogoliubov spectrum for a homogeneous Bose gas

$$\begin{aligned} \epsilon_k &= \sqrt{E_k\big(E_k + 2n\left(g + V_d(\mathbf{k})\right)\big)} \\ &= \sqrt{E_k\big(E_k + 2gn\left(1 + \epsilon_{dd}(3\cos^2\theta_k - 1)\right)\big)} \end{aligned} \tag{2.26}$$

where $E_k = \hbar^2k^2/2m$ is the kinetic energy, θ_k is the angle between the dipole orientation and the direction of the propagation of the excitation and we have defined

$$\epsilon_{dd} = \frac{g_d m}{3\hbar^2 a} = \frac{a_{dd}}{a} \tag{2.27}$$

with a_{dd} as the 'dipolar length' analogous to the s-wave scattering length. ϵ_{dd} is a measure of the dipolar strength relative to the contact interactions and has to be non-negligible in order to observe dipolar effects. However, note that when $\epsilon_{dd} \gtrsim 1$, the 3D homogenous gas is unstable against collapse. This can be seen from Eq. 2.26 as the phonons (low momentum excitations) have imaginary frequencies. This is known as the phonon instability and is direction dependent for dipolar condensates, contrary to the non-dipolar case which is isotropic and occurs when $g < 0$.

The spectrum Eq. 2.26 is obtained for a three dimensional condensate. Following the procedure of dimensional reduction(see Sec. 2.1.4), we can obtain the spectrum for a quasi 1D dipolar condensate [26]

$$\epsilon(q) = \hbar\omega = \sqrt{E_q\left(E_q + 2gn_0 + \frac{2g_d n_0}{3}F_0(ql_\rho)\right)} \tag{2.28}$$

where

$$F_0(q) = 1 + \frac{3}{2}q^2 e^{q^2/2}\mathrm{Ei}(-q^2/2) \tag{2.29}$$

with $\mathrm{Ei}(-q^2/2)$ as the exponential integral function. The spectrum 2.28 is plotted in Fig. 2.4 for representative values of the parameters. We see that the spectrum for a non-dipolar gas($g_d = 0$) is monotonous and tends to the free-particle regime at high momenta. For low momenta, the excitations are collective in nature and behave as phonons $\epsilon_k \sim k$. In contrast, the spectrum for a dipolar gas can be non-monotonous where the energy is linear for low momenta(phonons) and for higher momenta, there is a maximum in energy(maxon) followed by a minimum(roton). This is the celebrated roton-maxon spectrum[2] which was first discovered in dipolar condensates for an infinite quasi 2D dipolar condnesate with dipoles perpendicular to the trap plane [58]. However, this is due to the attractive nature of the DDI at large momenta, $V_d(\mathbf{k}) < 0$ for $k > 1/l_z$ where l_z is the harmonic oscillator length. The roton in Fig. 2.4 is due to $g < 0$ which is why it occurs for much smaller momenta. When the roton touches zero and the energy becomes imaginary, the condensate becomes

---

[2] This was first proposed by Landau in the context of superfluid ^{4}He [56, 57]

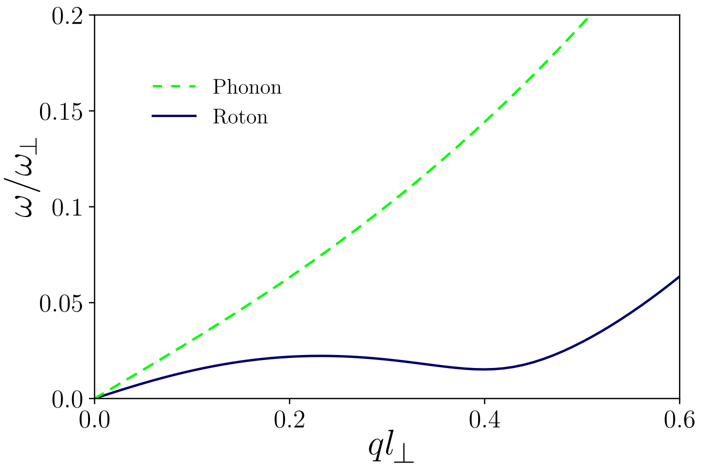

Figure 2.4: Excitation spectra for a quasi one dimensional non-dipolar(green dashed line) and dipolar(blue solid line) condensate. The spectrum for a non-dipolar gas is monotonous whereas the spectrum for a dipolar condensate is non-monotonous for chosen parameters.

unstable. This is known as the roton instability and is qualitatively different from the phonon instability discussed previously.

Experimental observation of roton mode

The roton mode was first experimentally observed in Ref. [60], where they used Bragg spectroscopy to study the momentum distribution of BECs of highly magnetic ^{166}Er atoms in a cigar shaped geometry with the dipoles oriented along one of the tightly confined directions. They also studied the instability dynamics of the roton mode by quenching the contact interaction parameter(s-wave scattering length) to a regime where the roton mode had imaginary energy(roton instability described above). Subsequently, Ref. [59] measured the rotonic excitation spectrum in a stable dipolar condensate of ^{166}Er using the method of Bragg spectroscopy following a number of theoretical proposals to measure the excitation spectrum [61–63]. The dynamic structure factor $S(q,\omega)$ is a measure of the response of a condensate to a Bragg pulse and turns out to be an excellent probe for the excitation spectrum(see Fig. 2.5) with an enhancement of the response of the condensate when the frequency and momenta of the Bragg pulse are close to that of the roton mode. Recently, Ref. [64] studied the roton excitations in a ^{162}Dy BEC by an analysis of the *in situ* density fluctuations. They could directly measure the static structure factor $S(k)$, which shows a

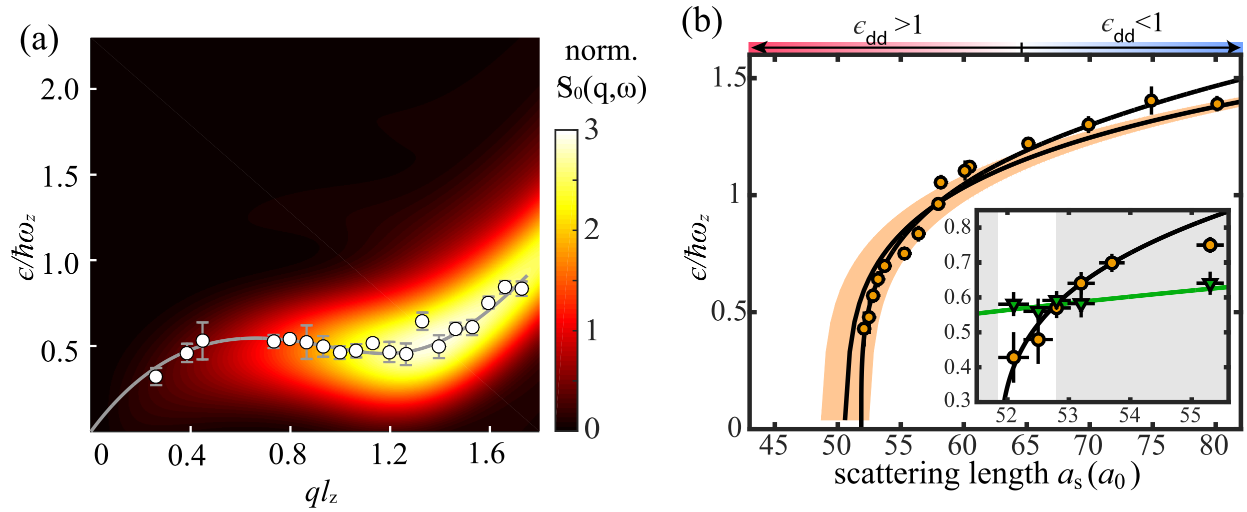

Figure 2.5: Roton excitation spectrum of a ^{166}Er cigar shaped dBEC. (a) Measured dispersion relation(dots) along with the predicted dynamic structure factor from Bogoliubov theory(colorcode).(b) Measured $\epsilon(k_{rot})$ vs scattering length(circles). The solid line shows the theoretical prediction with the shading denoting the calculations for the prediction interval of a_s. Inset shows the comparison of $\epsilon(k_{rot})$(circles) and $\epsilon(k_{max})$(triangles). The figure is taken from [12, 59].

maximum in the presence of a roton and diverges where the roton softens(roton instability). This further confirms that the density-density correlations are enhanced in the presence of a roton. The static structure factor can be related to the excitation spectrum through a particularly simple formula known as the Feynman-Bijl formula,

$$S(k) = \frac{E(k)}{\epsilon(k)} \tag{2.30}$$

where $E(k)$ is the kinetic energy and $\epsilon(k)$ is the dispersion relation. Eq. 2.30 makes it easy to see why there is a maximum in the static structure factor when there is a roton in the excitation spectrum.

2.2 Faraday patterns

Faraday instability is a type of modulation instability that occurs when a parameter in the system is periodically modulated. Faraday waves were first observed by Michael Faraday on

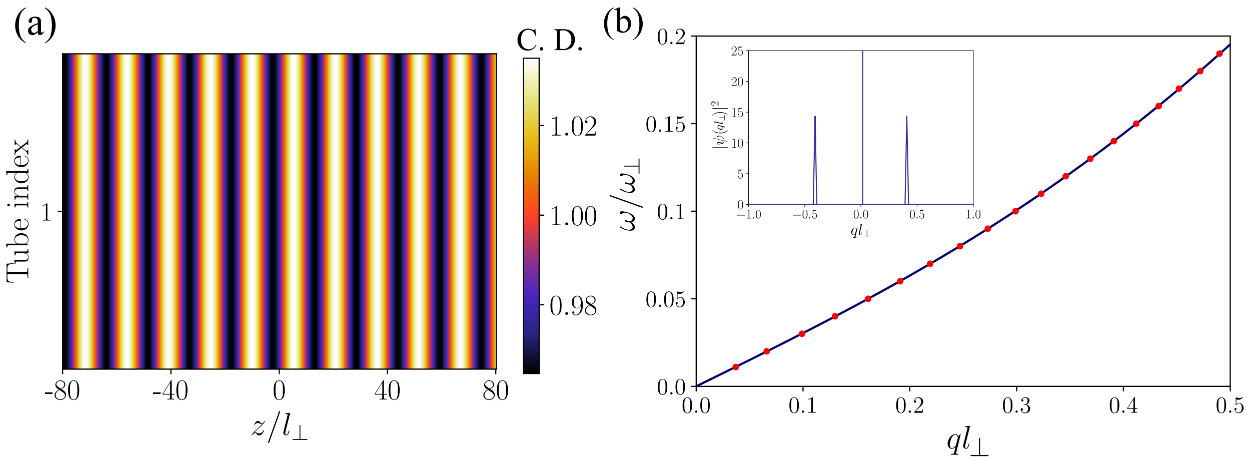

Figure 2.6: (a) Faraday pattern in a quasi one dimensional non-dipolar condensate. The wave number q of the pattern satisfies $\hbar\omega_m = \epsilon(q)$ where ω_m is the modulation frequency and $l_\perp$ is the harmonic oscillator length. (b) Filled circles(red) show the most unstable momentum as a function of the modulation frequency for the phonon spectrum in Fig. 2.4. Numerically, the most unstable momentum has a peak in the momentum space density, as shown in the inset for the pattern in (a). For (a), we have taken a finite width in the transverse direction for better visualization. C. D. denotes condensate density.

the surface of a vibrating liquid subjected to transverse oscillations. The patterns oscillate at half the frequency of the driving frequency. The type of the pattern depends on the system under consideration and can include stripes, squares, hexagonals, spirals and so on. The wave numbers of the patterns satisfy the dispersion relation $\omega_m = \omega(k)$ where $2\omega_m$ is the modulation frequency, and in more complicated systems, there can be multiple wave numbers that constitute pattern formation.

In Bose-Einstein condensates, Faraday patterns have been studied theoretically as well as experimentally by modulating the non-linearity in the condensates. The periodic driving includes the parametric modulation of the s-wave scattering length [4, 10, 65–67] or the modulation of the transverse trap frequency [68–70], leading to the growth of the instabilities and formation of patterns on top of the condensate. Floquet analysis can be used to study pattern formation, which reveals that the excitations can be written as $f(t)e^{\sigma t}$ where σ is known as the Floquet/Mathieu characteristic exponent and $f(t)$ is a periodic function. The Mathieu exponent σ is complex in general, and $\text{Re}(\sigma) > 0$ indicates the instability of the condensate against periodic driving, and the excitations grow exponentially. The dominant wave number corresponds to $\max(\text{Re}(\sigma))$ and is determined by the excitation spectrum of the

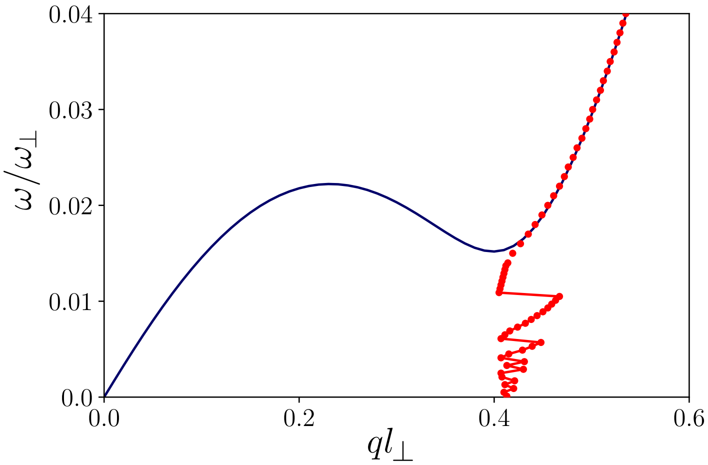

Figure 2.7: Non-trivial wave number selection in dipolar condensates with a roton-maxon spectrum. The red solid line shows the most unstable momentum as a function of driving frequency for the rotonic spectrum in Fig. 2.4. The roton leads to a cut off in the most unstable momenta by making the higher harmonics more unstable, contrary to the phonon case in Fig. 2.6.

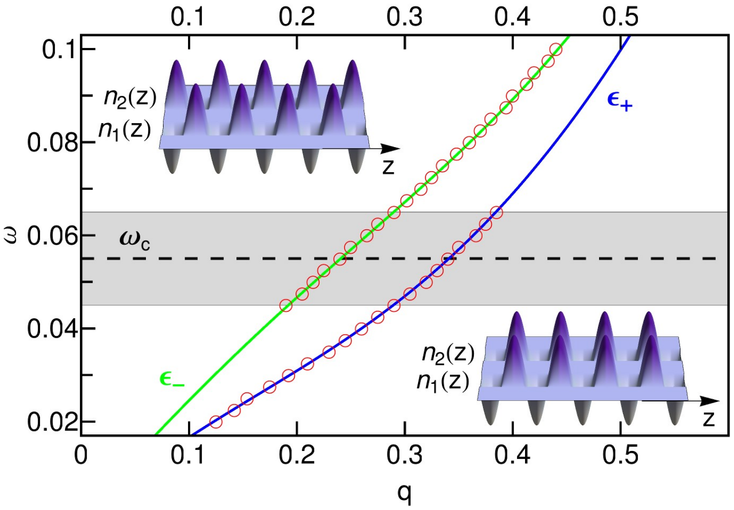

Figure 2.8: Pattern selection as a function of driving frequency. The solid lines correspond to excitation branches. The circles indicate the most unstable momenta for a given driving frequency. For driving frequency above a critical frequency, the most unstable modes correspond to anti-symmetric patterns whereas for lower frequencies, the most unstable mode represent symmetric patterns. The figure is taken from [26].

condensate through parametric resonances $n\hbar\omega_m = \epsilon(q)$ for small modulation amplitudes, similar to the classical case. In non-dipolar gases, the first harmonic($n = 1$) has the largest $\text{Re}(\sigma)$ and $\sigma \sim q^2$, which means that the wave number of the patterns increases monotonously with the driving frequency as the spectrum is monotonous(see Fig. 2.6).

Faraday patterns have also been studied in dipolar condensates in quasi 2D [71] and quasi 1D geometries [26, 72, 73]. The presence of the roton-minimum significantly modifies the wave number selection for dipolar condensates. For a given range of the modulation frequency $\omega_{roton} < \omega_m < \omega_{maxon}$, there are now three unstable modes $q_1 < q_2 < q_3$ instead of the single unstable mode in scalar BECs. Which mode is the most unstable depends on the details of the system. For a quasi 2D dipolar BEC, it was found in Ref. [71] that the most unstable mode corresponds to the intermediate momentum $q_2 < q_{roton}$.

Faraday patterns in a pair of quasi one dimensional dipolar condensates was explored in [26]. The long-range nature of the dipolar interactions leads to collective excitations in the pair of condensates. Consequently, the Bogoliubov spectrum splits into two branches corresponding to in phase and out of phase density modulations. The parametric modulation of the dipolar strength g_d leads to excitation of the modes and the most unstable mode corresponds to the one with the larger momentum $q_3 > q_{roton}$. Additionally, in the presence of a roton, the higher harmonics $n = 2, 3, \ldots$ become more unstable at lower modulation frequencies, thereby leading to a cutoff in the wave number of the patterns as shown in Fig. 2.7. Interestingly, they also observed a transition from a symmetric(in phase) Faraday pattern to an anti-symmetric(out of phase) pattern as the modulation frequency is increased(see Fig. 2.8).

Faraday patterns have also been studied in other Bose-Einstein condensate systems, such as multi-component non-dipolar BECs [74, 75]. In Ref. [74], they studied pattern formation in binary Bose-Einstein condensates via parametric modulation. They observed oscillatory patterns at the interface of the immiscible condensates when the scattering length of the inner condensate was periodically varied. In Ref. [75], upon periodic modulation of the radial confinement, they observed Faraday waves and two experimentally relevant stationary-state configurations. Pattern formation in spin-orbit coupled BECs was studied in Ref. [76], where they observed density and spin waves due to the spin-orbit coupling and a quench of the relative phase of two lasers. Faraday patterns have also been observed in spinor Bose-Einstein condensates [77, 78]. In Ref. [78], they observed a competition between density pattern and spin-mixing dynamics.

Chapter 3

Setup and Bogoliubov excitations

In this chapter and the next one we shall discuss the results of [30]. We shall study a stack of quasi one-dimensional dipolar BECs subjected to periodically varying s-wave scattering length. We shall begin by describing the non-linear GPEs governing the dynamics. We will then move on to study the Bogogliubov excitation spectrum and show that we can engineer the lowest-lying Bogoliubov mode by changing the dipole orientation. The lowest Bogoliubov mode determines the nature of the patterns and it can be engineered to be *in* phase or *out* of phase density modulations between the neighbouring condensates depending on whether the inter-tube dipolar interaction is attractive or repulsive respectively.

3.1 Setup

We study a stack of N homogenous, quasi one-dimensional dipolar BECs as shown in Fig. 3.1. The condensates form an array along the y direction. The distance between neighbouring condensates Δ is chosen such that there is no overlap between the condensates. For reference, the overlap between two neighbouring condensates separated by $\Delta = 5l_\perp$ is of the order 10^{-3} assuming a gaussian width in the transverse directions whereas for $\Delta = 6l_\perp$, the overlap is of the order 8×10^{-4} and $l_\perp = \sqrt{\hbar/m\omega_\perp}$ is the harmonic oscillator length with $\omega_\perp$ as the harmonic trapping frequency in the transverse directions. The condensates experience strong harmonic confinement in the x and y directions and no confinement in the z direction. The dipoles are polarized in the xy plane, making an angle ϕ with the y-axis. The intra-tube

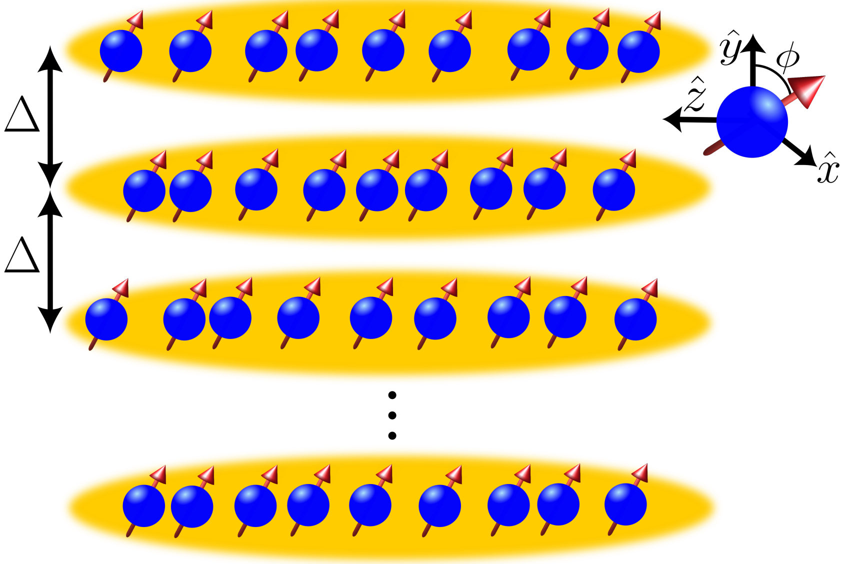

Figure 3.1: The schematic setup of a stack of Q1D dipolar BECs. The angle ϕ, between the dipole moment and the y-axis (in the plane), determines the nature of inter-tube DDIs, and Δ is the separation between the adjacent condensates along the y-axis.

dipolar interactions are always repulsive while the inter-tube interactions are attractive for $\phi = 0$ and repulsive for $\phi = 90$ degrees. The dipoles have a dipole moment d; the results are equally valid for magnetic or electric dipoles. The three dimensional Gross-Pitaevskii equations describing the condensates in each tube are

$$i\hbar\frac{\partial\Psi_j(r,t)}{\partial t} = \left[-\frac{\hbar^2}{2M}\nabla^2 + g_{3D}|\Psi_j(r,t)|^2 + \sum_{m=1}^{N}\int dr' n_m(r')V_d(r-r')\right]\Psi_j(r,t), \tag{3.1}$$

where $\Psi_j(r,t)$ is the wave function of the jth condensate. The parameter $g_{3D} = 4\pi\hbar^2 a_s/m$ quantifies the short-range interaction strength with a_s being the s-wave scattering length. $V_d(r) = g_d(1-3\cos^2\theta)/r^3$ is the dipole-dipole interaction potential where $g_d \propto \mu^2$ provides the strength of the DDIs and θ is the angle between the dipole orientation and the separation vector $\mathbf{r}$ between two dipoles. Due to the strong harmonic confinement, we can assume that the condensates remain in the ground state of the harmonic oscillator in the x and y directions(single mode approximation) given by

$$\phi_j^{\perp}(x,y) = \frac{1}{\sqrt{\pi}l_\perp}e^{-\frac{1}{2l_\perp^2}\left(x^2+(y-j\Delta)^2\right)} \tag{3.2}$$

such that $\Psi_j(r,t)$ can be separated as $\Psi_j(r,t) = \phi_j^{\perp}(x,y)\psi_j(z,t)$. We then multiply both sides with $\phi_j^{\perp *}(x,y)$ and integrate over the x and y directions to obtain a set of coupled non-local Gross-Pitaevskii equations(NLGPEs) that describe the system at very low temperatures,

$$i\hbar\frac{\partial\psi_j(z)}{\partial t} = \left[-\frac{\hbar^2}{2M}\frac{\partial^2}{\partial z^2} + gn_j(z) + \frac{g_d}{3}\sum_{l=1}^{N}\int\frac{dq}{2\pi}e^{iqz}n_l(q)F_{|l-j|}(q)\right]\psi_j(z), \tag{3.3}$$

where $\psi_j(z)$ is the wave function of the jth condensate, $n_j(z) = |\psi_j(z)|^2$ is the density of the jth condensate. $g = \frac{g_{3D}}{2\pi l_\perp^2}$ is the 1D contact interaction strength, $n_l(q)$ is the Fourier transform of the condensate density, and

$$F_p(q,\phi) = \int_0^\infty dk\frac{ke^{-\frac{1}{2}k^2l_\perp^2}}{k^2+q^2}\left[(k^2-2q^2)J_0(pk\Delta) - 3k^2\cos{(2\phi)}\,J_2(pk\Delta)\right], \tag{3.4}$$

It can be easily seen from Eq. 3.4 that $F_0(k)$ which represents intra-tube dipolar interactions is independent of ϕ as expected and $F_{p\neq 0}(k)$ representing inter-tube interactions depends on ϕ. $J_n(x)$ is the Bessel function of the first kind. The quasi 1D nature of the condensates requires that $\mu_j \ll \hbar\omega_\perp$, $\forall j$ where μ_j is the chemical potential of the jth condensate. The calculation to obtain $F_p(q,\phi)$ is briefly outlined below. First, we rewrite the dipolar term in the momentum space using the convolution theorem,

$$\int d\mathbf{r}V_d(\mathbf{r}-\mathbf{r}')|\Psi(\mathbf{r}',t)|^2 = \int\frac{d\mathbf{k}}{(2\pi)^3}e^{i\mathbf{k}.\mathbf{r}}V_d(\mathbf{k})|\Psi(\mathbf{k},t)|^2 \tag{3.5}$$

where $V_d(\mathbf{k})$ is the Fourier transform of the dipole-dipole potential and is given by,

$$V_d(\mathbf{k}) = \frac{4\pi}{3}g_d\left(\frac{3k_x^2\sin^2\phi + 3k_xk_y\sin 2\phi + 3k_y^2\cos^2\phi}{k_x^2+k_y^2+k_z^2} - 1\right) \tag{3.6}$$

We then integrate over x and y and convert the remaining integral to cylindrical coordinates $k_x = k\sin\theta$ and $k_y = k\cos\theta$ to obtain the form of Eq. 3.4.

3.2 Bogoliubov spectrum

In this section we calculate the Bogoliubov excitation spectrum to be able to identify the stability and the behaviour of the excitations. We consider the Bogoliubov ansatz discussed previously(refer Secs.2.1.5) - we consider a homogeneous ground state due to no confinement along z, and plane-wave like excitations

$$\psi_j(z,t) = e^{-i\mu t/\hbar}\left[\sqrt{n_0} + u_j e^{-i(qz-\omega t)} + v_j^* e^{i(qz-\omega t)}\right] \tag{3.7}$$

where n_0 is the linear density of the condensate, u_j and v_j^* are the quasiparticle amplitudes for particles and holes respectively. Substituting the above ansatz in the coupled GPEs and linearizing in the quasiparticle amplitudes, we obtain the corresponding Bogoliubov de Gennes equations for the excitations,

$$\begin{aligned}(gn_0 + E_q)\, u_j + gn_0 v_j + \frac{g_d n_0}{3}\sum_{l=1}^{N} F_{|l-j|}(q)[u_l + v_l] &= \hbar\omega_j u_j \\ (gn_0 + E_q)\, v_j^* + gn_0 u_j^* + \frac{g_d n_0}{3}\sum_{l=1}^{N} F_{|l-j|}(q)[u_l^* + v_l^*] &= -\hbar\omega_j v_j^*\end{aligned} \tag{3.8}$$

It can be seen from Eq. 3.8 that the excitations are collective in nature due to the dipole-dipole interactions(see Fig. 3.4) and there are N number of solutions for N numberof layers. For two layers, the spectrum splits into two branches corresponding to *in* phase and *out* of phase density modulations,

$$\epsilon_\pm(q) = \hbar\omega_\pm = \sqrt{E_q\left(E_q + 2gn_0 + \frac{2g_d n_0}{3}(F_0(ql_\perp) \pm F_1(ql_\perp))\right)} \tag{3.9}$$

The spectrum for two layers is plotted in Figure 3.2 for $\phi = 0$ and $\phi = 90$ degrees and for different parameter regimes. As discussed previously, the dipole-dipole interactions are attractive for $\phi = 0$ and the lowest Bogoliubov mode corresponds to *in* phase density modulations whereas the dipolar interactions are repulsive for $\phi = 90$ degrees and the density modulations are *out* of phase between neighbouring condensates. As we increase the dipole angle from 0 degrees, the magnitude of the dipolar interactions as well as the attractive nature decrease and reach a minimum at the 'magic angle'($\phi = \cos^{-1}(1/\sqrt{3})$). Further increasing the dipole angle increases the magnitude, however the interactions are repulsive and reach a maximum at 90 degrees.

When the excitation energy is real and a monotonic function of the momentum, the spectrum is said to be phononic; when the energy is real but non-monotonous, the spectrum is rotonic and when the energy is imaginary, it is said to have a roton instability if the unstable momenta are finite, and the condensates have a phonon instability if the instability

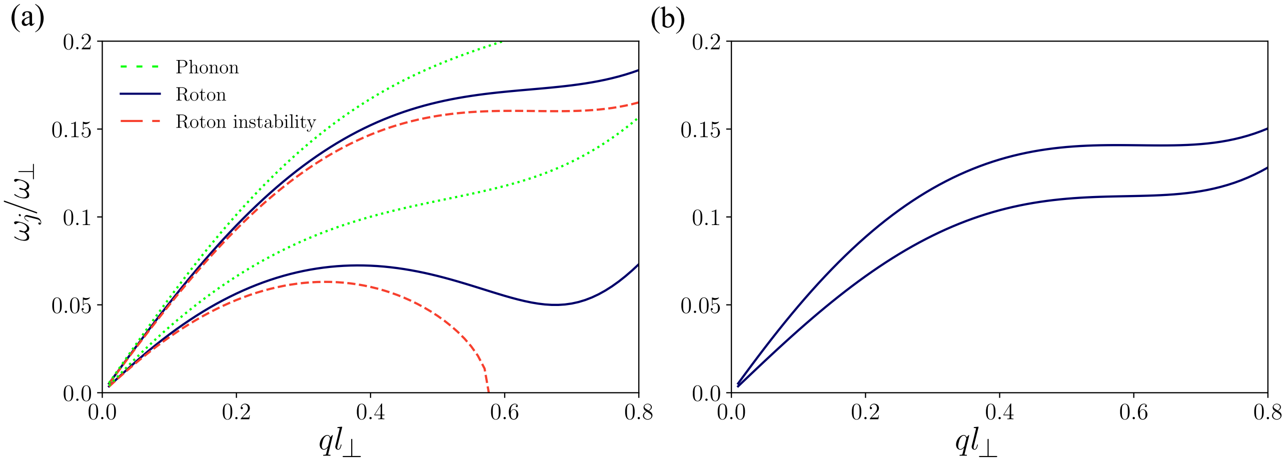

Figure 3.2: Bogoliubov excitation spectra for two layers. (a) $\phi = 0$ with i. phonon $gn_0 = -0.06\hbar\omega_\perp$ (green dotted line) ii. roton $gn_0 = -0.09\hbar\omega_\perp$(blue solid line) iii. roton instability $gn_0 = -0.1\hbar\omega_\perp$(red dashed line). (b) $\phi = 90$ degrees. $g_d n_0 = 0.14\hbar\omega_\perp$ and $\Delta = 5l_\perp$ in all the plots.

occurs at zero momentum. We can go from one regime to another by making g increasingly negative keeping other parameters fixed or by increasing g_d, thereby increasing the strength of the dipolar interactions. However, we cannot increase g or g_d beyond a point as the quasi one-dimensional character breaks down.

The BdG equations 3.8 are generally solved numerically because although analytical expressions for the excitation energies can be obtained in principle, the expressions become too complicated to be useful after $N = 4$. We can rewrite the BdG equations in the form of a matrix equation and the problem reduces to an eigenvalue problem making it easier to handle. In general, for N layers the BdG matrix is $2N \times 2N$ dimensional and the matrix equation is given by,

$$\begin{pmatrix} b_d & b_0 & \dots & b_{n-1} & b_{n-1} \\ -b_0 & -b_d & \dots & -b_{n-1} & -b_{n-1} \\ & & \ddots & & \\ b_{n-1} & b_{n-1} & \dots & b_d & b_0 \\ -b_{n-1} & -b_{n-1} & \dots & -b_0 & -b_d \end{pmatrix} \begin{pmatrix} u_1 \\ v_1 \\ \vdots \\ u_n \\ v_n \end{pmatrix} = \hbar\omega \begin{pmatrix} u_1 \\ v_1 \\ \vdots \\ u_n \\ v_n \end{pmatrix}$$

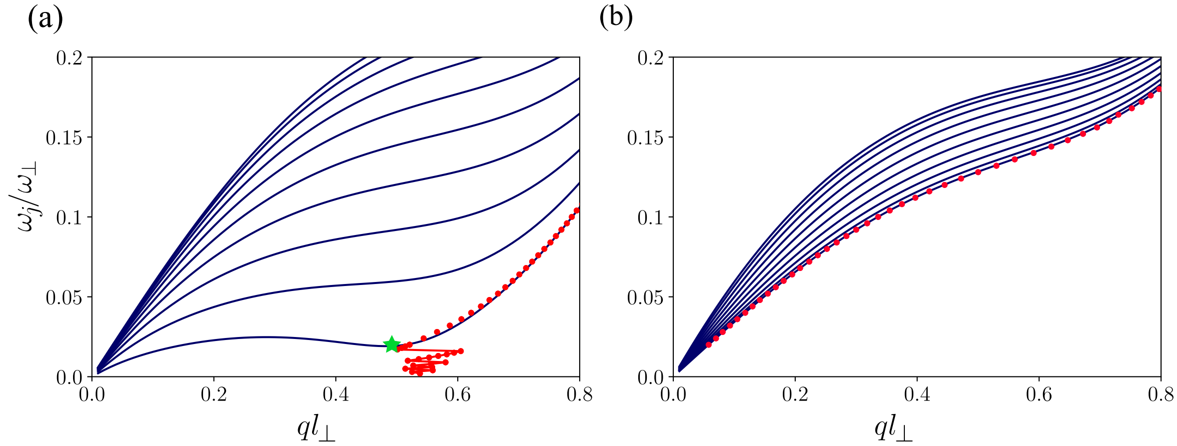

Figure 3.3: Bogoliubov spectrum of ten Q1D homogeneous dipolar condensates with $gn_0 = -0.06\hbar\omega_\perp, gdn_0 = 0.14\hbar\omega_\perp$, and $\Delta = 5l_\perp$ with the dipole orientation (a) $\phi = 0$ degrees and (b) $\phi = 90$ degrees. Filled circles (red) show the most unstable momentum for the amplitude of modulation $\alpha = 0.06$ as an increasing function of driving frequency ω_m (refer Sec. 4.1), which follows the lowest branch. In (a), the roton minimum (marked by a star) causes a nontrivial wavenumber selection when $\omega_m < \omega_r$, where ω_r is the roton mode frequency. In particular, the higher harmonics such that $n\omega_m \gtrapprox \omega_r$ with $n = 2, 3, \dots$ become more unstable, putting a lower bound to the unstable momenta appearing in the system

where we have defined

$$\begin{aligned} b_d &= E_q + gn_0 + \frac{g_d n_0}{3} F_0(ql_\perp) \\ b_0 &= gn_0 + \frac{g_d n_0}{3} F_0(ql_\perp) \\ b_m &= \frac{g_d n_0}{3} F_m(ql_\perp) \end{aligned} \tag{3.10}$$

We plot the Bogoliubov spectrum for ten Q1D condensates in Figure 3.3 for both orientations. The spectra have ten branches and the character of the lowest mode depends on dipole orientation. The spectrum for $\phi = 0$ is sparse and has a roton minimum(note that this is because we have $g < 0$) whereas the spectrum is dense for $\phi = 90$ degrees. The parameters used are the same as the ones that give a phonon spectrum for two layers. This property is known as roton softening(not be confused with the terminology for when roton frequency touches zero which can be considered as a special case) where, for the same parameters, the roton mode frequency keeps decreasing on increasing the number of layers; and eventually, the system enters the roton instability regime. For the parameters used in the figure 3.3, this occurs when we have $N = 13$(see Fig. 3.5). In what follows, we have restricted the

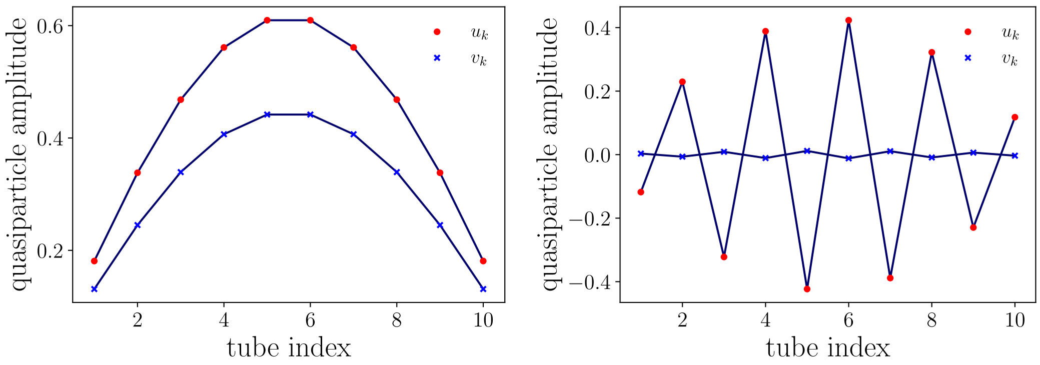

Figure 3.4: Quasiparticle amplitudes for the lowest Bogoliubov mode at $ql_\perp = 0.5$ for (a) $\phi = 0$ and (b) $\phi = 90$ degrees. The modes are collective in nature and have contributions from all the tubes. The amplitudes in (a) are in phase whereas the amplitudes of the neighbouring condensates are out of phase with each other in (b).

parameters such that the spectrum is purely real and the Lee–Huang–Yang (LHY) quantum correction to the chemical potential from quantum fluctuations can be neglected [79, 80].

Effect of increasing the number of tubes

We take a detour to mention what happens when we increase the number of tubes. We have discussed the case when the dipoles are oriented head-to-tail($\phi = 0$). In this case the roton frequency decreases as we increase the number of tubes and eventually the system develops roton instability where the homogenous ground state is dynamically unstable. On the other hand, when the dipoles are side-by-side($\phi = 90$ degrees) the spectrum becomes denser as we increase the number of tubes(see Fig. 3.5) and as we shall discuss in the next section, multiple Bogoliubov modes become equally(nearly) unstable and grow simultaneously. This leads to a superposition of patterns with many unstable momenta.

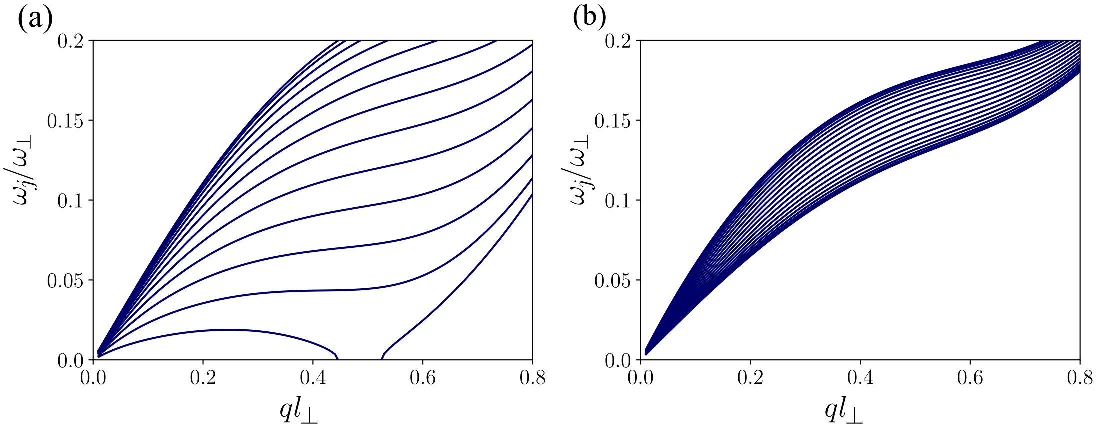

Figure 3.5: Effect of increasing the number of layers on the Bogoliubov spectrum. (a) $N = 13$, $\phi = 0$ degrees and (b) $N = 20$, $\phi = 90$ degrees. In (a), a roton instability develops and grows deeper as we further increase the number of layers. In (b) the spectrum is dense and leads to a superposition of patterns when periodically driven. The parameters used are $gn_0 = -0.06\hbar\omega_\perp, gdn0 = 0.14\hbar\omega_\perp$, and $\Delta = 5l_\perp$.

Chapter 4

Stripe and checkerboard patterns

We have seen in the previous chapter that we can engineering the lowest Bogoliubov mode to correspond to in phase and out of phase density modulations by changing the dipole orientation. In this chapter, we shall see that the parametric modulation of the s-wave scattering length induces stripe(*in* phase) or checkerboard(*out* of phase) density patterns depending on the dipole angle. Further, we shall discuss the dynamics of quenching the dipole angle once the initial pattern has formed via periodic driving. The results discussed here are from [30].

4.1 Parametric driving

In this section, we consider the parametric modulation of the s-wave scattering length. This can be achieved experimentally via the modulation of the magnetic field near a Feshbach resonance which leads to a modulation of the scattering length. The scattering length is modulated as,

$$a_s(t) = \bar{a}_s[1 + 2\alpha \cos(2\omega_m t)] \tag{4.1}$$

where α is the strength of the modulation and ω_m is the modulation frequency. This leads to the growth of the instabilities in the system and consequently leads to density modulations. To understand the pattern selection, we consider the following solution to the coupled GPEs in Eq. 3.3, $\psi_j(z,t) = \psi_j^H(z,t)\left[1 + K_j(t)\cos qz\right]$ where

$$\psi_j^H(z,t) = \sqrt{n_0}\exp\left(-i\left[\frac{\mu_j t}{\hbar} + \frac{\alpha\bar{g}n_0}{\hbar\omega_j}\sin(2\omega_m t)\right]\right) \tag{4.2}$$

is the homogeneous solution in the presence of periodic modulation and $\bar{g} = \frac{2\hbar^2\bar{a}_s}{ml_\perp^2}$. $K_j(t) = r_j(t) + is_j(t)$ is the complex amplitude of the density modulation. We replace this ansatz in Eq. 3.3 and only retain the terms that are linear in $K_j(t)$. This is justified since we are assuming small amplitude modulations and the higher-order terms can be ignored. We then separate the real and imaginary terms to get,

$$\begin{aligned} \hbar\frac{dr_j}{dt} &= \frac{\hbar^2 q^2}{2m}s_j \\ -\hbar\frac{ds_j}{dt} &= \frac{\hbar^2 q^2}{2m}r_j + 2g(t)n_0 + \frac{2}{3}g_d\sum_{l=1}^{N}F_{|l-j|}(q)r_l \end{aligned} \tag{4.3}$$

The coupled equations above can be combined into a single second-order equation which reads,

$$\hbar^2\frac{d^2r_j}{dt^2} + E_q\left[E_q + 2g(t)n_0\right]r_j + \frac{2}{3}g_dE_q\sum_{l=1}^{N}F_{|l-j|}(q)r_l = 0, \tag{4.4}$$

We again rewrite the above equation in terms of a matrix equation

$$\hbar^2\frac{d^2\mathcal{R}(t)}{dt^2} + \mathcal{A}\mathcal{R}(t) = 0 \tag{4.5}$$

where $\mathcal{A} = E_q\left[E_q + 2g(t)n_0\right]\mathbb{I} + \mathcal{G}(q)$, $\mathbb{I}$ is a $N \times N$ identity matrix and $\mathcal{R} = (r_1, r_2, \ldots r_N)^T$. The matrix $\mathcal{G}(q)$ is given by,

$$\mathcal{G}(q) = \frac{2}{3}g_dE_q\begin{pmatrix} F_0(q) & F_1(q) & \ldots & F_{N-1}(q) \\ F_1(q) & F_0(q) & \ldots & F_{N-2}(q) \\ F_2(q) & F_1(q) & \ldots & F_{N-3}(q) \\ \vdots & \vdots & \vdots & \ddots \end{pmatrix}. \tag{4.6}$$

where $F_p(q)$ is given in Eq. 3.4. Finally, we can decouple Eq. 4.5 into N independent Mathieu-like equations,

$$\hbar^2 \frac{d^2 \bar{r}_j}{dt^2} + \left[\epsilon_j^2(q) + 4\alpha \bar{g} n_0 E_q \cos(2\omega_m t)\right] \bar{r}_j = 0, \tag{4.7}$$

where $\bar{r}_j = \mathbf{g}_j^T \mathcal{R}$ is the collective modulation amplitude of the stack of dipolar Q1D condensates with $\mathbf{g}_m$ being the mth eigenvector of $\mathcal{A}$ and $\epsilon_j(q) = \hbar\omega_j$ is the Bogoliubov dispersion. Note that the index j in $\epsilon_j(q)$ refers to the Bogoliubov mode and not the layer index. Refer to Appendix A for the details of the calculations.

Floquet theory

Floquet theory is a branch of Ordinary Differential equations that deals with periodic linear differential equations of the form $\dot{x} = A(t)x$ where $A(t+T) = A(t)$ is a periodic function with period T. The main result of Floquet's theorem is that we can define a coordinate change $y = B^{-1}(t)x$ with $B(t+2T) = B(t)$ such that the above equation can be transformed into a tradition linear differential equation with constant coefficients. Its application to Mathieu equations gives the result that the solutions of the Mathieu equations are of the form $f(t)e^{\sigma t}$ where $f(t + \frac{\pi}{\omega}) = f(t)$ is a periodic function and σ is called the Floquet/Mathieu exponent. The real part of the Floquet exponent is known as the Lyapunov exponent in non-linear dynamics. The solutions are said to be Lyapunov stable if the Lyapunov exponents are non-negative and unstable if they are positive.

In our system, the solutions of Eq. 4.7 take the form $\bar{r}_j(t) = f_j(t)e^{\sigma_j t}$ where $f_j(t) = f_j(t + \pi/\omega_m)$. $\mathrm{Re}(\sigma) > 0$ indicates the dynamical instability of the condensates to the periodic modulation and leads to the growth of transient Faraday patterns before they are eventually destroyed. In the limit of small modulation amplitudes $\alpha \to 0$, the pattern selection is determined by the resonances $n\hbar\omega = \epsilon_j(q)$, $\forall j$. The solution with the largest $\mathrm{Re}(\sigma)$ grows the fastest and hence dominates the dynamics. If the condensates are driven for a long time, all the modes become more and more unstable leading to larger and larger excitations before the condensates are inevitably destroyed and out of the mean-field regime.

For a phonon spectrum and for the first harmonic($n = 1$), there are N unstable momenta and the one corresponding to the lowest branch will be the most unstable. Hence, the most unstable momenta follows the lowest branch in the Bogoliubov spectrum. In contrast, for

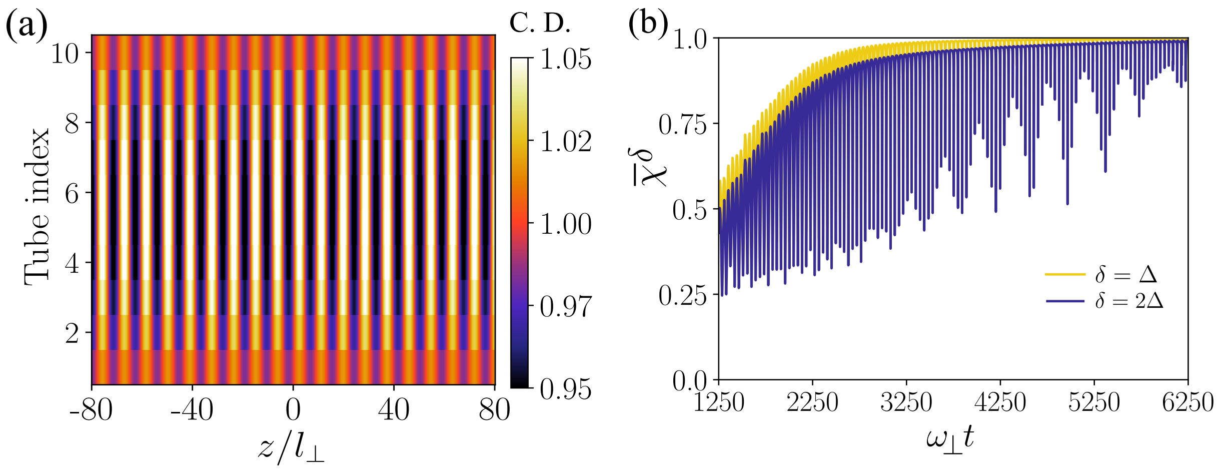

Figure 4.1: (a) Stripe density pattern and (b) the corresponding density-density correlations in a stack of ten Q1D dipolar condensates for $\phi = 0$ degrees, $gn_0 = -0.06\hbar\omega_\perp$, $g_d n_0 = 0.14\hbar\omega_\perp$, $\Delta = 5l_\perp$, $\alpha = 0.01$ and $\omega_m = 0.07\omega_\perp$. The snapshot of the pattern is taken at $\omega_\perp t = 6185$. The average density-density correlation $\bar{\chi}^\delta$ is shown for nearest ($\delta = \Delta$) and next-nearest condensates ($\delta = 2\Delta$). While plotting, we have taken a finite width of the condensate along the transverse y-direction for better visualization. C.D. stands for condensate density.

a roton spectrum and the first harmonic, the number of unstable momenta will be higher due to the presence of the roton in a given range of frequency $\omega_{roton} < \omega_m < \omega_{maxon}$. The most unstable momenta now depends on the geometry of the condensates as we discussed previously.
When the modulation frequency $\omega_m < \omega_{roton}$, the situation is more involved if the spectrum has a roton mode. The higher harmonics $n = 2, 3, \ldots$ start to play a role in pattern selection and hence the most unstable momentum acquires a non-trivial character.

We now discuss the numerical study of the time evolution of the coupled GPEs(Eq. 3.3) under periodic modulation and the observation of transient density patterns.

4.1.1 Stripe pattern

We first consider the case of the dipoles oriented along y-axis($\phi = 0$ degrees). The inter-tube interactions are attractive, and the lowest Bogoliubov mode has symmetric character. We consider the case in Fig. 3.3 (a) which has a roton minimum in the lowest branch which is marked by a star. The periodic modulation leads to the growth of instablities and as we have seen, the lowest mode is the most unstable. The excitation of the lowest mode leads to stripe density pattern as shown in Fig. 4.1, where we have shown the numerical results for ten condensates. We also show the wave function density of the central condensate in momentum space in Fig. 4.3. The wave function shows a central peak at $k = 0$ corresponding to the condensate and two other symmetric peaks corresponding to the excited modes. The momenta corresponding to the peak satisfy the resonance condition $\epsilon_j(q) = \hbar\omega$. We see from Fig. 4.1 that the central condensates have a larger amplitude than the outer condensates due to the finite number of tubes. Consequently, the contrast between the high and low density regions is also lower for the outer condensates. As discussed previously, the presence of roton leads to non-trivial wave number selection. The first harmonic is the most unstable for $\omega_m > \omega_r$, whereas for $\omega_m < \omega_r$, the higher harmonics having energy closer to the roton are more unstable.

To quantify the nature of the pattern, we calculate the density-density correlation between a pair of condensates,

$$\chi^{(j,k)}(t) = \frac{\int dz S_j(z,t) S_k(z,t)}{\sqrt{\left(\int dz\ S_j^2(z,t)\right)}\sqrt{\left(\int dz\ S_k^2(z,t)\right)}} \tag{4.8}$$

where $S_j(z,t) = n_j(z,t) - n_0$ with n_j denoting the density of the jth tube along the y-axis. Experimentally, these correlations can be measured from the simultaneous in situ imaging of the density of all tubes [64, 81, 82]. The average density-density correlation among all pairs of tubes separated by a distance δ is defined as,

$$\bar{\chi}^{\delta}(t) = \frac{1}{N - \delta/\Delta} \sum_{j=1}^{N-\delta/\Delta} \chi^{(j,j+\delta/\Delta)}(t). \tag{4.9}$$

We plot the average density-density correlation between nearest($\delta = \Delta$) and next-nearest neighbouring condensates for the stripe pattern in Fig. 4.1(b). Since the density modulations are in phase, $\bar{\chi}^{\delta}$ is positive irrespective of δ. $\bar{\chi}^{\delta} = 1$ indicates maximal correlation and we see that the correlations tend to one for the stripe pattern. We also observe oscillations in the correlations $\bar{\chi}^{\delta}$ due to the oscillations in the amplitude with the frequency ω_m. The maximum value of the correlation also decreases with increase in δ as can be expected since the effect of the dipolar interactions decreases.

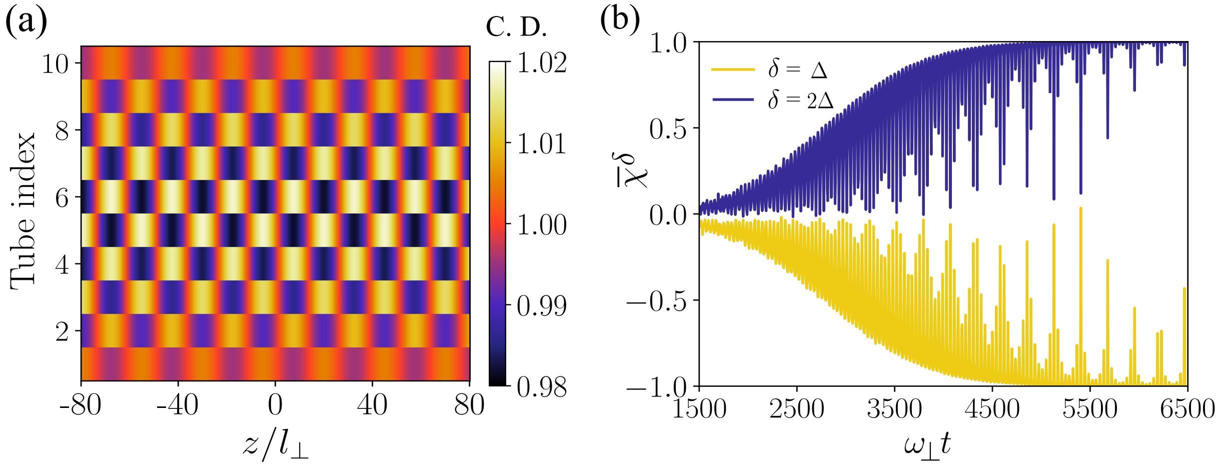

Figure 4.2: (a) Checkerboard density pattern and (b) the corresponding density-density correlations in a stack of ten Q1D dipolar condensates for $\phi = 90$ degrees, $gn_0 = -0.06\hbar\omega_\perp$, $g_d n_0 = 0.14\hbar\omega_\perp$, $\Delta = 5l_\perp$, $\alpha = 0.06$ and $\omega_m = 0.08\omega_\perp$. The snapshot of the pattern is taken at $\omega_\perp t = 6500$. We have taken a finite width of the condensate along the transverse y-direction for better visualization. The average density-density correlation $\bar{\chi}^\delta$ is shown for nearest ($\delta = \Delta$) and next-nearest condensates ($\delta = 2\Delta$). C.D. stands for condensate density.

Effect of noise: We embed a tiny uniform random noise($\sim 10^{-4}$) on top of the homogeneous density(~ 1) in the condensate wave function at the start of the simulation to seed the instabilities. Increasing the magnitude to the noise leads to decrease in the correlations and also the time taken to form the density patterns. We need to be careful as a high value of noise can lead to a high value of the kinetic energy at the start which may break down the quasi 1D nature assumed.

4.1.2 Checkerboard pattern

We now consider dipoles oriented along x-axis($\phi = 90$ degrees). The lowest Bogoliubov mode corresponds to anti-correlated density modulations between the neighbouring condensates and its excitation leads to a checkerboard pattern as shown in Fig. 4.2. The spectrum is monotonous and hence the most unstable momentum follows the lowest Bogoliubov branch(see Fig. 3.3). The Fourier space density is plotted in Fig. 4.3 and shows two peaks(apart from the condensate peak) characterizing the excited momenta. Since the density modulations between the neighbouring condensates are out of phase, the nearest

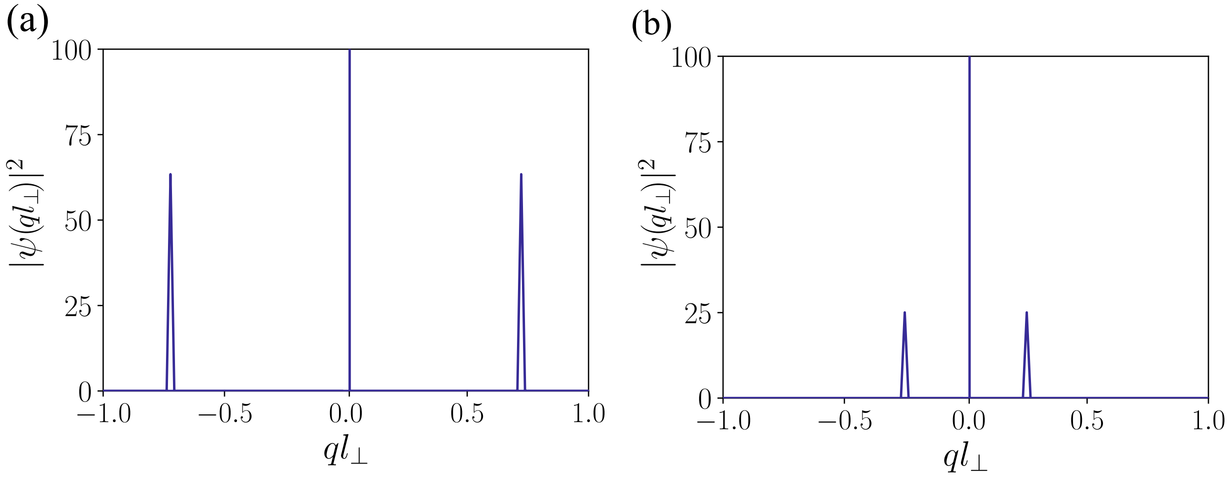

Figure 4.3: Momentum space density for (a) Stripe pattern($\phi = 0$ degrees) and (b) checkerboard pattern($\phi = 90$ degrees). The peaks at at the momenta satisfying the resonance condition $\epsilon_j(q) = \hbar\omega_\perp$ for the lowest branch and the first harmonic since $\omega_m > \omega_r$. The snapshots are taken at (a) $\omega_\perp t = 6185$ and (b) $\omega_\perp t = 6500$. The parameters used are (a) $\alpha = 0.01$ and $\omega = 0.07\omega_\perp$, (b) $\alpha = 0.06$ and $\omega = 0.08\omega_\perp$. Other parameters are $gn_0 = -0.06\hbar\omega_\perp$, $g_d n_0 = 0.14\hbar\omega_\perp$, $\Delta = 5l_\perp$.

neighbour correlation $\bar{\chi}^{\delta=\Delta} \to -1$ whereas the next-nearest neighbour density modulations are in phase, hence leading to $\bar{\chi}^{\delta=2\Delta} \to 1$ at intermediate times. The behaviour of $\bar{\chi}^{\delta}$ can be summarized as negative correlations for condensates separated by odd multiples of Δ and positive correlations for condensates separated by even multiples of Δ. We again observe oscillations in $\bar{\chi}^{\delta}(t)$ with frequency ω_m.

Stripe vs checkerboard patterns: In addition to the differences we discussed above, the stripe and checkerboard patterns differ in terms of the time taken to form/have a significant amplitude. This is evident from the Figs. 4.1, 4.2 and 4.3 as the strength of modulation in the case of checkerboard pattern is higher and yet, the amplitude of the density pattern around the same time as the stripe pattern is smaller. This can be attributed to the fact that the dipolar interactions are twice as strong in the stripe case compared to the checkerboard case and hence stripe patterns grow faster.

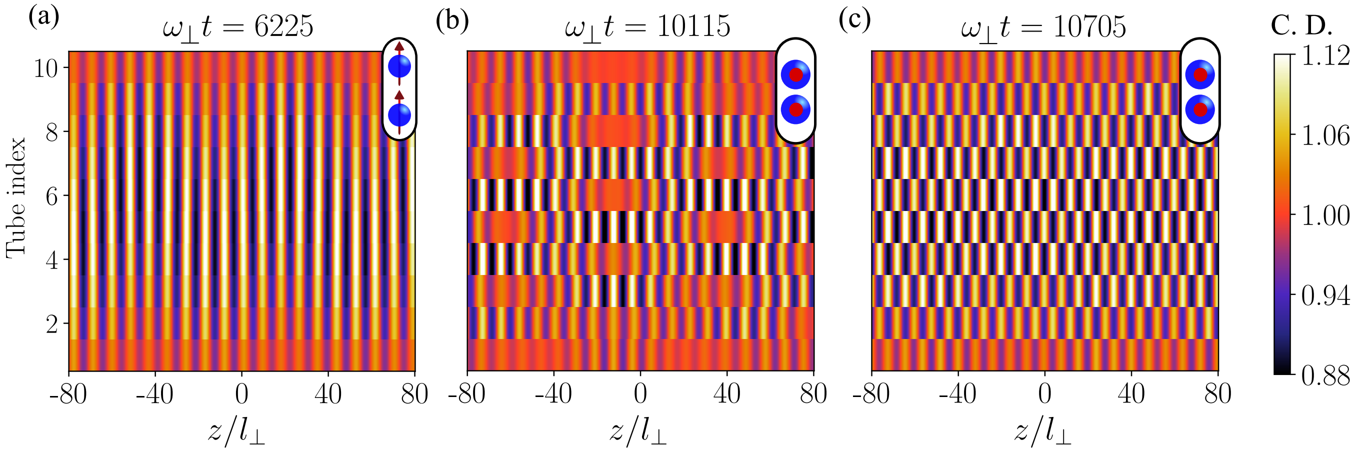

Figure 4.4: Stripe to checkerboard transition upon instantaneous quench of dipole angle. ϕ is quenched from $0 \to 90$ degrees. The time for each snapshot is shown at the top of each plot. $\omega_m = 0.07\omega_\perp$ and $\alpha = 0.01$ before we quench at $\omega_\perp t = 6250$, The dipole orientation is shown at the top right for each plot. Other parameters are $gn_0 = -0.06\hbar\omega_\perp$, $g_d n_0 = 0.14\hbar\omega_\perp$, and $\Delta = 5l_\perp$.

4.2 Abrupt quench

We periodically modulate the scattering length until the stripe or the checkerboard pattern is formed. We then simultaneously stop the periodic driving and abruptly quench the dipole angle. There are two possible scenarios - i. We initially form the stripe pattern($\phi = 0$) and quench the angle to $\phi = 90$ degrees. ii. We first create the checkerboard pattern($\phi = 90$ degrees) and immediately quench the angle to $\phi = 0$ degrees. Interestingly, we observe a dynamic transition between the two patterns, and their dynamics differ significantly. We'll first describe the stripe to checkerboard transition.

4.2.1 Stripe to checkerboard transition

We first form the stripe pattern by periodic driving 4.4(a). We then stop the periodic driving simultaneously quench ϕ to 90 degrees. The qeuenching makes the stripes unstable as the dipole angle changes from $\phi = 0$ degrees(maximally attractive) to $\phi = 90$ degrees(maximally repulsive). The stripes eventually break apart 4.4(b) and align themselves into the checkerboard pattern as shown in Fig. 4.4(c). This dynamical transition can be described by the density-density correlation coefficient which is plotted in Fig. 4.5. For the stripe to checkerboard transition, $\bar{\chi}^{\delta=\Delta}$ corresponding to nearrest-neighbour correlations, changes from a maximum value of 1 indicating maximal positive correlations, to a value of -1 indicating the neighbouring condensates are maximally anti-correlated and the patterns transition to checkerboard. Note that $\bar{\chi}^{\delta=2\Delta}$ representing next-nearest neighbour correlations remains positive throughout.

Interestingly, we observe that the time taken for the patterns to transition is dependent on various factors. All parameters being the same, the transition time is different even for a different noise realization. The amplitude of patterns at a given time varies from realization to realization and the maximum amplitudes of the condensate wave functions oscillate in time with frequency ω_m due to the periodic driving while there is an overall exponential increase in time. We found that the time taken for transition depends critically on the maximum amplitude of the pattern before the quenching. We verified this by observing the dynamics for a large number of different noise realizations. The relevant quantity is the maximum amplitude before quenching and not the amplitude at the instant of quenching. The transition time is higher for a low amplitude of the patterns before quenching and if the amplitude is very low, there may not be a transition at all.

In order to quantify our observations we calculated the energy functional for our system. We defined the energy functional for a dipolar gas in Eq. 2.18. We plot the normalized energies in Fig. 4.6 where we have normalized by the (box size×number of tubes). We can see from the figure that the kinetic energy increases exponentially before the quench after which it oscillates and increases during the transition. This increase can be attributed to the motion of the density peaks during the transition. Corresponding to the increase in kinetic energy, there has to be a decrease in other energies as we have stopped the periodic driving and are no longer supplying energy to the system. This decrease can be seen in the contact and dipolar energies(Fig. 4.6(b) and (c)). Thus there is a critical amplitude to observe the transition for a given set of parameters. Also note that in the long time limit, other modes become unstable leading to the destruction of the patterns and eventually the condensate.

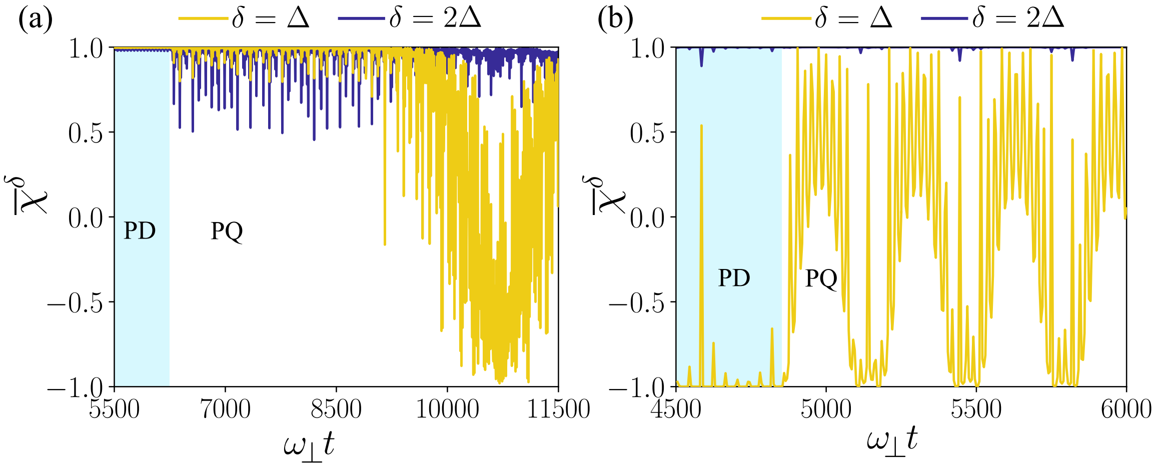

Figure 4.5: Average density-density correlation $\bar{\chi}^{\delta}(t)$ for the abrupt quench. (a) Stripe to checkerboard transition($\phi = 0$ to $\phi = 90$ degrees). and (b) checkerboard to stripe transition($\phi = 90$ to $\phi = 0$ degrees). The modulation parameters are (a) $\omega = 0.07\omega_{\perp}$ and $\alpha = 0.01$ before the quench at $\omega_{\perp} t = 6250$ and (b) $\omega = 0.08\omega_{\perp}$, $\alpha = 0.08$ before the quench at $\omega_{\perp} t = 4850$. Other parameters are same as Fig. 4.4. PD stands for periodic driving and PQ stands for post-quench.

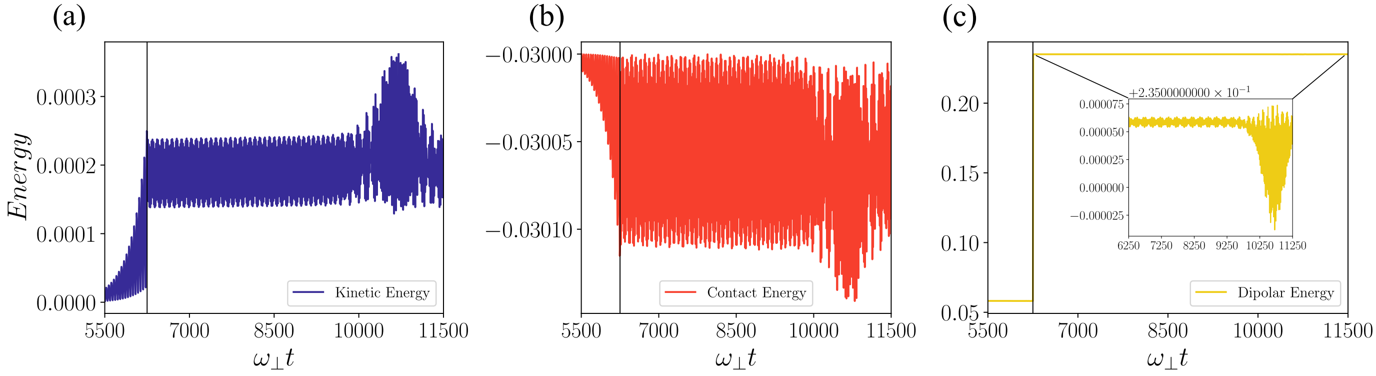

Figure 4.6: Normalized energy plots for the stripe to checkerboard transition. (a) Kinetic energy (b) Contact energy and (c) dipolar energy. The time of the quenching is shown by a black solid vertical line. The inset in (c) shows the zoomed in plot of dipolar energy during the transition. The kinetic energy increases during the transition whereas the contact and dipolar energies decrease.

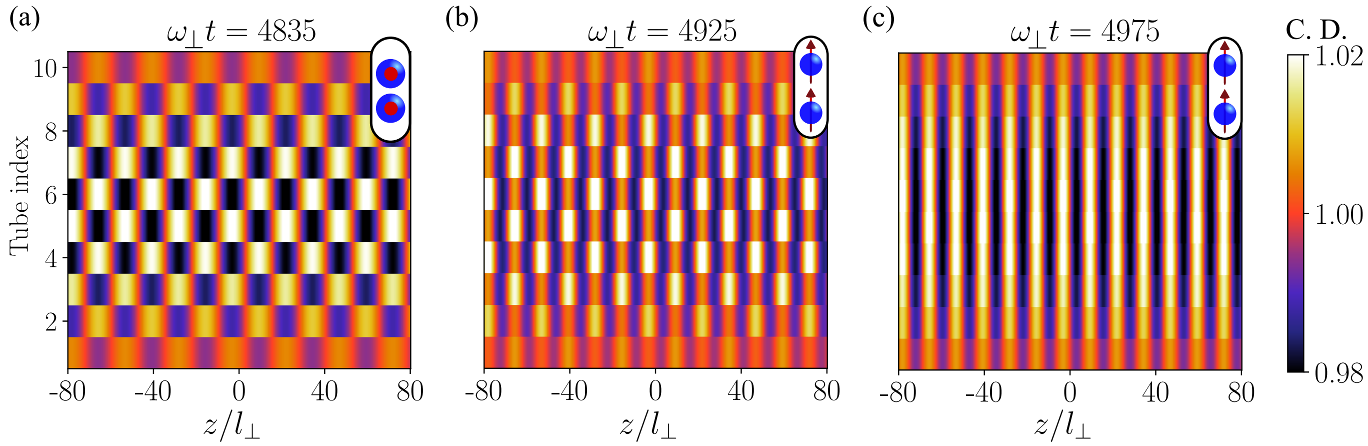

Figure 4.7: Checkerboard to stripe transition. ϕ is quenched from 90 → 0 degrees. The time for each snapshot is shown at the top of each plot. $\omega_m = 0.08\omega_\perp$ and $\alpha = 0.08$ before we quench at $\omega_\perp t = 4850$, The dipole orientation is shown at the top right for each plot. Other parameters are the same as Fig. 4.4.

4.2.2 Checkerboard to stripe transition

Periodic modulation of the scattering length at $\phi = 90$ degrees leads to a checkerboard pattern Fig. 4.7(a). Abruptly changing the dipole angle to 0 changes the dipolar interactions to maximally attractive making the checkerboard unstable. Each of the density peaks in the checkerboard pattern splits into two due to the attraction from the density peaks on either sides in the neighbouring tubes, eventually forming a stripe pattern(see Fig. 4.7(b) and (c)). As the density peaks split to form the stripe pattern, the periodicity of the stripe pattern is half that of the initial checkerboard. The corresponding density-density correlations are shown in Fig. 4.5(b). We see that the pattern transition occurs almost immediately, which is contrary to the stripe to checkerboard transition. This can be explained as follows - the strength/magnitude of the inter-tube dipolar interactions when the dipoles are head-to-tail($\phi = 0$) is twice as strong when they are side-by-side($\phi = 90$ degrees). Hence, upon quenching the dipolar interactions become stronger and the transition happens immediately. We can also see from Fig. 4.5(b) that the nearest neighbour correlation $\bar{\chi}^{\delta=\Delta}$ changes from -1 to a value of 1 after the quench and oscillates between the two. This is also seen in the density patterns as they oscillate between checkerboard and stripe patterns. The next-nearest neighbour correlation $\bar{\chi}^{\delta=2\Delta} \sim 1$ throughout.

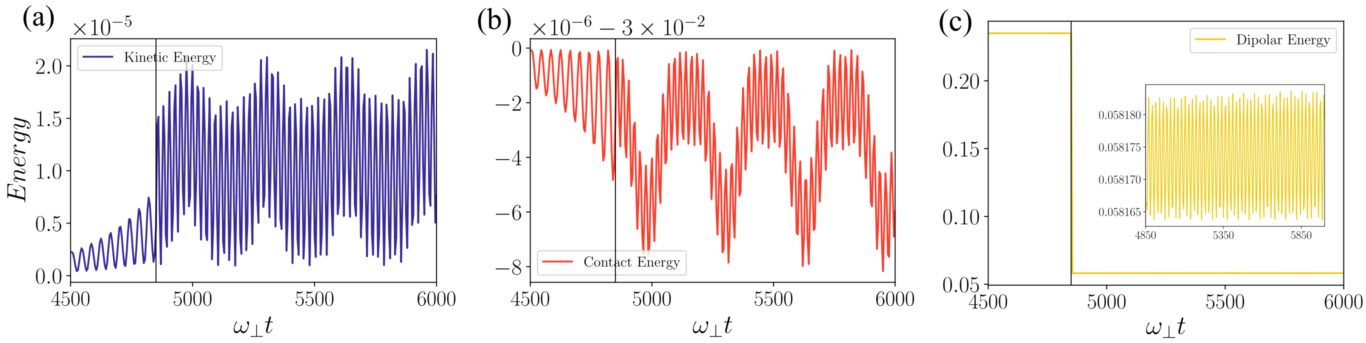

Figure 4.8: Normalized energy plots for the checkerboard to stripe transition. (a) Kinetic energy (b) Contact energy and (c) dipolar energy. The time of the quenching is shown by a black solid vertical line. The inset in (c) shows the zoomed in plot of dipolar energy during the transition. The kinetic and contact energies oscillate out of phase with each other during the transitions, whereas the dipolar energy oscillates without change throughout.

The normalized energies are plotted in Fig. 4.8. The kinetic energy increases exponentially before the quench and oscillates with the modulation frequency ω_m. The kinetic and contact energies oscillate out of phase with each other after the quench meaning the contact energy is transferred to the kinetic energy and vice versa. The dipolar energy oscillates with no change during the transitions. We also observed that when the amplitude of the patterns before quenching was very high, the condensates get destroyed almost immediately after the quench

4.3 Linear quench

The quenching of the dipolar angle can be implemented experimentally by varying the magnetic field. However, this means that the abrupt quench may be difficult to achieve in practice. Therefore, we numerically study a linear quench of the dipole angle to see if the transitions still occur. We periodically drive the condensates until we obtain the stripe or checkerboard pattern as before. We then stop the periodic driving and quench the dipole angle in steps of one degree every few time steps. We plot the correlation coefficients for the transitions in Fig. 4.9. We see that there is no qualitative change in the dynamics; however, the transition time has increased as the dipolar interactions take longer time to become attractive/repulsive. We also verified that the qualitative dynamics remains the same if we

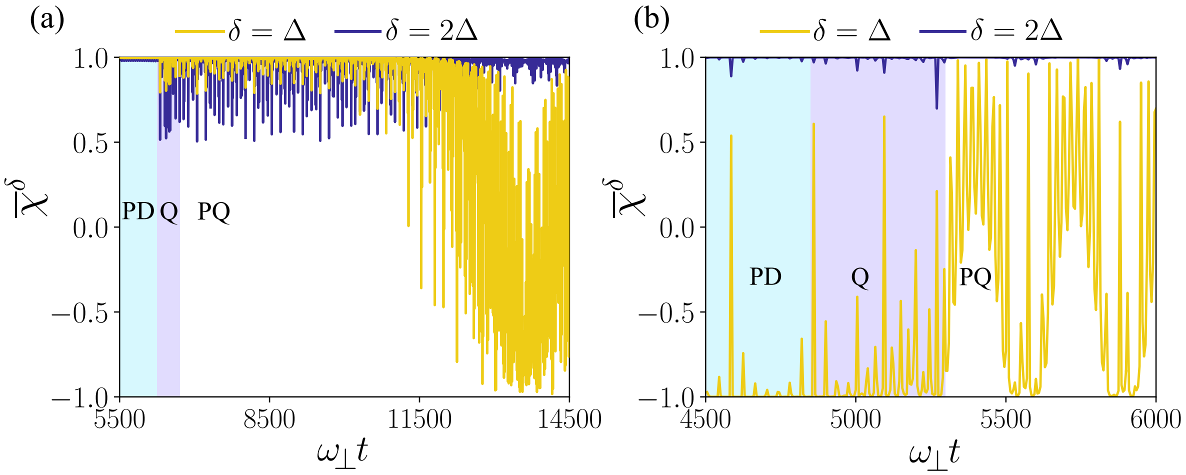

Figure 4.9: Average density-density correlation $\bar{\chi}^{\delta}(t)$ for the linear quench of the dipole angle. (a) stripe to checkerboard transition($\phi = 0$ to $\phi = 90$ degrees) and (b) checkerboard to stripe transition($\phi = 90$ to $\phi = 0$ degrees). The parameters are the same as Fig. 4.5. In (a) the quench starts at $\omega_{\perp}t = 6250$ and ends at $\omega_{\perp}t = 6695$ and in (b) from $\omega_{\perp}t = 4850$ to $\omega_{\perp}t = 5295$. The dipole angle is changed in increments of one degree every $\omega_{\perp}t = 5$. The total time of quench is $89\omega_{\perp}t = 445$. PD denotes periodic driving, Q for the regime of the linear quench and PQ for postquench.

change the quench rate; however note that a very slow quench can lead to suppression of the vibrational modes of the pattern and a complete revival of the initial pattern may not be possible. The normailzed energies are plotted in Fig. 4.10. This further confirms that there is no qualitative change in the dynamics. As we discussed before, the amplitude of the patterns have to be above a threshold value for the transitions to occur. To illustrate this, we plot the average density-density correlations $\bar{\chi}^{\delta}$ in Fig. 4.11 for both cases where the transition is delayed/doesn't occur. The dynamics of the condensates remains the same before the quench. However, we now quench earlier than before to study the dynamics. We see from Fig. 4.11(a) for the stripe to checkerboard transition that the transition happens at a later time than before(see Fig. 4.9(a)) whereas in Fig. 4.11(b), the transition to the stripe pattern does not occur. Further, we verified that performing the quench at a later time leads to a transition.

We also performed simulations where we increased the dipole angle in steps of nine degrees and simulations with different quench rates which resulted in similar qualitative dynamics. Additionally, when we start from an intermediate angle $\phi = 45$ degrees and periodically drive the condensates, quenching the dipole angle to $\phi = 0$ results in a transition to a stripe pattern which gets destroyed quickly, and we did not observe a transition when we quenched

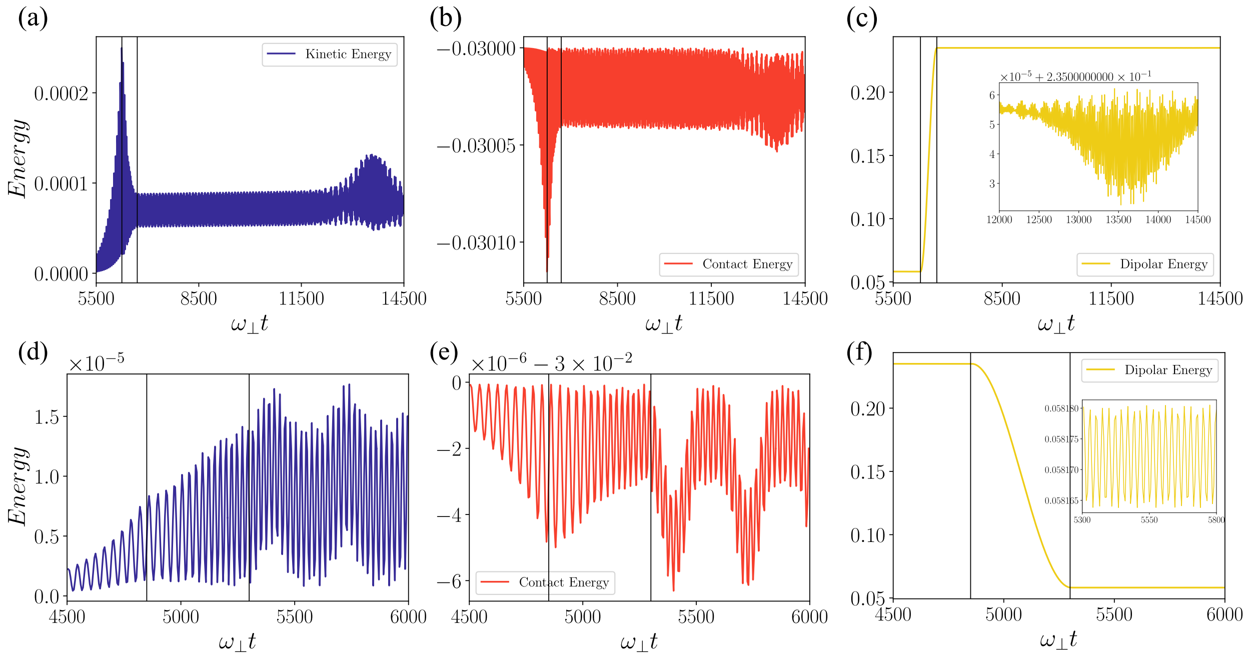

Figure 4.10: Normalized energy plots for the linear quench.(a)-(c) show the kinetic, contact and dipolar energies for the stripe to checkerboard transition. (d)-(f) show the same for the checkerboard to stripe transition. Notably, the kinetic energy decreases in (a) whereas it increases for (b). The qualitative properties remain the same while the transition time is prolonged.

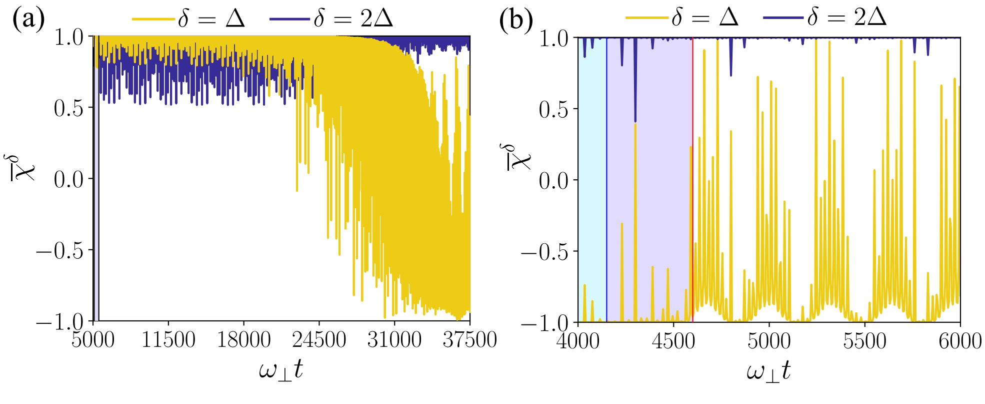

Figure 4.11: Effect of quenching the dipole angle earlier. (a) stripe to checkerboard transition and (b) checkerboard to stripe transition. The transition is delayed in (a) whereas it doesn't occur in (b).

the angle to 90 degrees(for a long time). This solidified our conjecture that the amplitude is the primary factor deciding the transition time.

Chapter 5

Summary and outlook

In this thesis, we studied stripe and checkerboard pattern formation in a stack of quasi one dimensional dipolar Bose-Einstein condensates upon parametric modulation of the s-wave scattering length. We showed that we can engineer the Bogoliubov spectrum via changing the orientation of the dipoles. The presence of inter-tube dipolar interactions leads to a collective nature of the excitations and the spectrum splits into different branches corresponding to different modes. The nature of the lowest mode can be engineered to be in phase or out of phase density modulations by changing the dipole orientation. The modulation of the s-wave scattering length leads to the excitation of the lowest Bogoliubov mode resulting in the observation of stripe and checkerboard patterns for attractive($\phi = 0$ degrees) and repulsive($\phi = 90$ degrees) dipolar inter-tube interactions respectively. The wave number selection can be analyzed through Mathieu-like equations and Floquet theory. The nature of the patterns can be described by average the density-density correlation coefficient $\bar{\chi}^{\delta}$ which tends to 1 for positive correlations and to -1 indicating anti-correlations. All the condensates are in phase in the stripe pattern resulting in $\bar{\chi}^{\delta} \sim 1$ whereas for checkerboard pattern, nearest neighbour condensates are out of phase $\bar{\chi}^{\delta=\Delta} \sim -1$ and next-nearest neighbours are in phase $\bar{\chi}^{\delta=2\Delta} \sim 1$.

We then study the dynamics of quenching the dipole angle once the initial pattern has formed via periodic driving. We observe a dynamical transition between the patterns upon quenching ϕ abruptly or linearly. The transition can be described by the average correlation coefficient $\bar{\chi}^{\delta}$ which changes from 1 to -1 for the stripe to checkerboard transition, and from

-1 to 1 for the checkerboard to stripe transition. The checkerboard to stripe transition occurs almost immediately upon quenching whereas the transition from stripe to checkerboard happens at a later time. The time taken for the transition depends primarily on the pattern amplitude before quenching, in addition to various other factors. Further, we calculated the energy functionals to support our results.

Our studies offer several prospects. One possible study would be to design schemes to selectively excite any given Bogoliubov mode. Another possibility would be to study the patterns at an arbitrary angle and the dynamics upon quenching different parameters. The study could also be extended to quasi two dimensional condensates and anti-parallel dipoles which could lead to novel perspectives. It would also be interesting to study the addition of dissipation and investigate the steady state patterns or the hysteresis.

Appendix A

Mathieu equations

We start with the following equation.

$$\hbar^2 \frac{d^2 r_j}{dt^2} + E_q \left[E_q + 2g(t)n_0\right] r_j + \frac{2}{3} g_d E_q \sum_{l=1}^{N} F_{|l-j|}(q) r_l = 0, \tag{A.1}$$

which can be written as,

$$\hbar^2 \frac{d^2 \boldsymbol{R}(t)}{dt^2} + \left(E_q \left[E_q + 2g(t)n_0\right] \mathbb{I} + \boldsymbol{G}\right) \boldsymbol{R}(t) = 0. \tag{A.2}$$

Here $\mathbb{I}$ is an $N \times N$ identity matrix, $\boldsymbol{R} = (r_1, r_2, \ldots r_N)^T$ and

$$\boldsymbol{G}(q) = \frac{2}{3} g_d E_q \begin{pmatrix} F_0(q) & F_1(q) & F_2(q) & \ldots \\ F_1(q) & F_0(q) & F_1(q) & \ldots \\ F_2(q) & F_1(q) & F_0(q) & \ldots \\ \vdots & \vdots & \vdots & \ddots \end{pmatrix}. \tag{A.3}$$

Uncoupling the set of equations

We write (A.1) as,

$$\hbar^2 \frac{d^2 \boldsymbol{R}(t)}{dt^2} = -\boldsymbol{\mathcal{A}} \boldsymbol{R}(t), \tag{A.4}$$

where matrix $\boldsymbol{\mathcal{A}} = E_q \left[E_q + 2g(t) n_0 \right] \mathbb{I} + \boldsymbol{G}$. Assume the matrix $\boldsymbol{\mathcal{A}}$ is diagonalizable. Then we obtain the following diagonal matrix as,

$$\Lambda = S^{-1} \mathcal{A} S \tag{A.5}$$

where the matrix S is given by,

$$S = \begin{pmatrix} \boldsymbol{g}_1 & \boldsymbol{g}_2 & \dots & \boldsymbol{g}_n \end{pmatrix} \tag{A.6}$$

Here, the column vector $\boldsymbol{g}_i$ is the i-th eigenvector of the matrix $\mathcal{A}$. Since $\mathcal{A}$ is a real symmetric matrix, S will be an orthogonal matrix, i.e. $S^{-1} = S^T$. We multiply S^{-1} on the right of the equation,

$$\hbar^2 \frac{d^2}{dt^2} \left[S^{-1} \boldsymbol{R}(t) \right] = -S^{-1} \mathcal{A} \boldsymbol{R}(t), \tag{A.7}$$

and then insert identity as SS^{-1} on the RHS.

$$\hbar^2 \frac{d^2}{dt^2} \left[S^{-1} \boldsymbol{R}(t) \right] = -S^{-1} \mathcal{A} S S^{-1} \boldsymbol{R}(t) = \Lambda S^{-1} \boldsymbol{R}(t) \tag{A.8}$$

We define $\bar{\boldsymbol{R}}(t) = S^{-1} \boldsymbol{R}(t) = S^T \boldsymbol{R}(t)$. Since,

$$S^T = \begin{pmatrix} \boldsymbol{g}_1^T \\ \boldsymbol{g}_2^T \\ \vdots \\ \boldsymbol{g}_n^T, \end{pmatrix} \tag{A.9}$$

where $\boldsymbol{g}_i^T$ are row vectors and transpose of the eigenvectors, we have the

$$\bar{\boldsymbol{R}}(t) = S^T \boldsymbol{R}(t) = \begin{pmatrix} \boldsymbol{g}_1^T \boldsymbol{R}(t) \\ \boldsymbol{g}_2^T \boldsymbol{R}(t) \\ \vdots \\ \boldsymbol{g}_n^T \boldsymbol{R}(t) \end{pmatrix} \tag{A.10}$$

We can see that $\bar{r}_i = \boldsymbol{g}_i^T \boldsymbol{R}(t)$ (which is a scalar) is a linear combination of r_i and is used as the new set of variables.

$$\hbar^2 \frac{d^2 \bar{\boldsymbol{R}}(t)}{dt^2} = -\Lambda \bar{\boldsymbol{R}}(t) \tag{A.11}$$

Since the Λ is diagonal, the new sets of variables are uncoupled from each other.

Eigenvectors of $\boldsymbol{G}$

Here we note that since $\mathcal{A} = E_q \left[E_q + 2g(t)n_0\right] \mathbb{I} + \boldsymbol{G}$, the eigenvectors of $\mathcal{A}$ and $\boldsymbol{G}$ are the same. It can be shown as follows,

$$\begin{aligned} \Lambda &= S^{-1}\mathcal{A}S \\ &= E_q \left[E_q + 2g(t)n_0\right] S^{-1}\mathbb{I}S + S^{-1}\boldsymbol{G}S \\ &= E_q \left[E_q + 2g(t)n_0\right] \mathbb{I} + S^{-1}\boldsymbol{G}S \end{aligned} \tag{A.12}$$

Since Λ and $\mathbb{I}$ are diagonal, $S^{-1}\boldsymbol{G}S$ is diagonal as well, implying that the set of eigenvectors are same of both $\mathcal{A}$ and $\boldsymbol{G}$. This also ensure that the eigenvectors $\boldsymbol{g}_i$ are time-independent, which is required for the previous set of derivation to be valid.

Relation to the Bogoliubov dispersion

The entries of the diagonal matrix Λ, say λ_i, are the eigenvalues of $\boldsymbol{\mathcal{A}}$. They can be written as,

$$\lambda_i = E_q \left[E_q + 2g(t)n_0 \right] + \mu_i \tag{A.13}$$

where μ_i are the eigenvalues of $\boldsymbol{G}$. It happen to be that the eigenvalues coincides with $\epsilon_j(q)$. This is checked explicitly and verified for the different set of interaction parameters.

References

[1] M. C. Cross and P. C. Hohenberg. “Pattern formation outside of equilibrium”. In: *Rev. Mod. Phys.* 65 (3 1993), pp. 851–1112. DOI: 10.1103/RevModPhys.65.851.

[2] André Eckardt, Tharanga Jinasundera, Christoph Weiss, and Martin Holthaus. “Analog of Photon-Assisted Tunneling in a Bose-Einstein Condensate”. In: *Phys. Rev. Lett.* 95 (20 2005), p. 200401. DOI: 10.1103/PhysRevLett.95.200401.

[3] F. Kh. Abdullaev, A. M. Kamchatnov, V. V. Konotop, and V. A. Brazhnyi. “Adiabatic Dynamics of Periodic Waves in Bose-Einstein Condensates with Time Dependent Atomic Scattering Length”. In: *Phys. Rev. Lett.* 90 (23 2003), p. 230402. DOI: 10.1103/PhysRevLett.90.230402.

[4] J. H. V. Nguyen, M. C. Tsatsos, D. Luo, A. U. J. Lode, G. D. Telles, V. S. Bagnato, and R. G. Hulet. “Parametric Excitation of a Bose-Einstein Condensate: From Faraday Waves to Granulation”. In: *Phys. Rev. X* 9 (1 2019), p. 011052. DOI: 10.1103/PhysRevX.9.011052.

[5] Hiroki Saito and Masahito Ueda. “Dynamically Stabilized Bright Solitons in a Two-Dimensional Bose-Einstein Condensate”. In: *Phys. Rev. Lett.* 90 (4 2003), p. 040403. DOI: 10.1103/PhysRevLett.90.040403.

[6] D. S. Jin, J. R. Ensher, M. R. Matthews, C. E. Wieman, and E. A. Cornell. “Collective Excitations of a Bose-Einstein Condensate in a Dilute Gas”. In: *Phys. Rev. Lett.* 77 (3 1996), pp. 420–423. DOI: 10.1103/PhysRevLett.77.420.

[7] M.-O. Mewes, M. R. Andrews, N. J. van Druten, D. M. Kurn, D. S. Durfee, C. G. Townsend, and W. Ketterle. “Collective Excitations of a Bose-Einstein Condensate in a Magnetic Trap”. In: *Phys. Rev. Lett.* 77 (6 1996), pp. 988–991. DOI: 10.1103/PhysRevLett.77.988.

[8] S. E. Pollack, D. Dries, R. G. Hulet, K. M. F. Magalhães, E. A. L. Henn, E. R. F. Ramos, M. A. Caracanhas, and V. S. Bagnato. "Collective excitation of a Bose-Einstein condensate by modulation of the atomic scattering length". In: *Phys. Rev. A* 81 (5 2010), p. 053627. DOI: 10.1103/PhysRevA.81.053627.

[9] V I Yukalov, A N Novikov, and V S Bagnato. "Formation of granular structures in trapped Bose–Einstein condensates under oscillatory excitations". In: *Laser Physics Letters* 11.9 (2014), p. 095501. DOI: 10.1088/1612-2011/11/9/095501.

[10] Zhendong Zhang, Kai-Xuan Yao, Lei Feng, Jiazhong Hu, and Cheng Chin. "Pattern formation in a driven Bose–Einstein condensate". In: *Nature Physics* 16.6 (2020), pp. 652–656. ISSN: 1745-2481. DOI: 10.1038/s41567-020-0839-3.

[11] T Lahaye, C Menotti, L Santos, M Lewenstein, and T Pfau. "The physics of dipolar bosonic quantum gases". In: *Reports on Progress in Physics* 72.12 (2009), p. 126401. DOI: 10.1088/0034-4885/72/12/126401.

[12] Lauriane Chomaz, Igor Ferrier-Barbut, Francesca Ferlaino, Bruno Laburthe-Tolra, Benjamin L Lev, and Tilman Pfau. "Dipolar physics: a review of experiments with magnetic quantum gases". In: *Reports on Progress in Physics* 86.2 (2022), p. 026401. DOI: 10.1088/1361-6633/aca814.

[13] M.A. Baranov. "Theoretical progress in many-body physics with ultracold dipolar gases". In: *Physics Reports* 464.3 (2008), pp. 71–111. ISSN: 0370-1573. DOI: 10.1016/j.physrep.2008.04.007.

[14] M. A. Baranov, M. Dalmonte, G. Pupillo, and P. Zoller. "Condensed Matter Theory of Dipolar Quantum Gases". In: *Chemical Reviews* 112.9 (2012), pp. 5012–5061. DOI: 10.1021/cr2003568.

[15] Nicolo Defenu, Tobias Donner, Tommaso Macri, Guido Pagano, Stefano Ruffo, and Andrea Trombettoni. "Long-range interacting quantum systems". In: *Rev. Mod. Phys.* 95 (3 2023), p. 035002. DOI: 10.1103/RevModPhys.95.035002.

[16] Matthias Rosenkranz, Yongyong Cai, and Weizhu Bao. "Effective dipole-dipole interactions in multilayered dipolar Bose-Einstein condensates". In: *Phys. Rev. A* 88 (1 2013), p. 013616. DOI: 10.1103/PhysRevA.88.013616.

[17] Andrej Junginger, Jörg Main, and Günter Wunner. "Variational calculations on multilayer stacks of dipolar Bose-Einstein condensates". In: *Phys. Rev. A* 82 (2 2010), p. 023602. DOI: 10.1103/PhysRevA.82.023602.

[18] S. Müller, J. Billy, E. A. L. Henn, H. Kadau, A. Griesmaier, M. Jona-Lasinio, L. Santos, and T. Pfau. "Stability of a dipolar Bose-Einstein condensate in a one-dimensional lattice". In: *Phys. Rev. A* 84 (5 2011), p. 053601. DOI: 10.1103/PhysRevA.84.053601.

[19] Ryan M. Wilson and John L. Bohn. "Emergent structure in a dipolar Bose gas in a one-dimensional lattice". In: *Phys. Rev. A* 83 (2 2011), p. 023623. DOI: 10.1103/PhysRevA.83.023623.

[20] Kazimierz Łakomy, Rejish Nath, and Luis Santos. "Soliton molecules in dipolar Bose-Einstein condensates". In: *Phys. Rev. A* 86 (1 2012), p. 013610. DOI: 10.1103/PhysRevA.86.013610.

[21] G. Guijarro, G. E. Astrakharchik, and J. Boronat. "Ultradilute Quantum Liquid of Dipolar Atoms in a Bilayer". In: *Phys. Rev. Lett.* 128 (6 2022), p. 063401. DOI: 10.1103/PhysRevLett.128.063401.

[22] M. Klawunn and L. Santos. "Hybrid multisite excitations in dipolar condensates in optical lattices". In: *Phys. Rev. A* 80 (1 2009), p. 013611. DOI: 10.1103/PhysRevA.80.013611.

[23] Chao-Chun Huang and Wen-Chin Wu. "Center motions of nonoverlapping condensates coupled by long-range dipolar interaction in bilayer and multilayer stacks". In: *Phys. Rev. A* 82 (5 2010), p. 053612. DOI: 10.1103/PhysRevA.82.053612.

[24] Aleksandra Maluckov, Goran Gligori ć, Ljup čo Had žievski, Boris A. Malomed, and Tilman Pfau. "High- and low-frequency phonon modes in dipolar quantum gases trapped in deep lattices". In: *Phys. Rev. A* 87 (2 2013), p. 023623. DOI: 10.1103/PhysRevA.87.023623.

[25] Kazimierz Łakomy, Rejish Nath, and Luis Santos. "Soliton molecules in dipolar Bose-Einstein condensates". In: *Phys. Rev. A* 86 (1 2012), p. 013610. DOI: 10.1103/PhysRevA.86.013610.

[26] Kazimierz Łakomy, Rejish Nath, and Luis Santos. "Faraday patterns in coupled one-dimensional dipolar condensates". In: *Phys. Rev. A* 86 (2 2012), p. 023620. DOI: 10.1103/PhysRevA.86.023620.

[27] Li Du, Pierre Barral, Michael Cantara, Julius de Hond, Yu-Kun Lu, and Wolfgang Ketterle. *Atomic physics on a 50 nm scale: Realization of a bilayer system of dipolar atoms*. 2023. arXiv: 2302.07209 `[cond-mat.quant-gas]`.

[28] Niccolò Bigagli, Claire Warner, Weijun Yuan, Siwei Zhang, Ian Stevenson, Tijs Karman, and Sebastian Will. "Collisionally stable gas of bosonic dipolar ground-state molecules". In: *Nature Physics* 19.11 (2023), pp. 1579–1584. ISSN: 1745-2481. DOI: 10.1038/s41567-023-02200-6.

[29] Niccolò Bigagli, Weijun Yuan, Siwei Zhang, Boris Bulatovic, Tijs Karman, Ian Stevenson, and Sebastian Will. *Observation of Bose-Einstein Condensation of Dipolar Molecules*. 2023. arXiv: 2312.10965 `[cond-mat.quant-gas]`.

[30] S Nadiger, SM. Jose, R Ghosh, I Kaur, and R Nath. "Stripe and checkerboard patterns in a stack of driven quasi-one-dimensional dipolar condensates". In: *Phys. Rev. A* 109 (3 2024), p. 033309. DOI: 10.1103/PhysRevA.109.033309.

[31] A. Einstein. "Quantentheorie des einatomigen idealen Gases". In: *Albert Einstein: Akademie-Vorträge*. John Wiley and Sons, Ltd, 2005, pp. 237–244. ISBN: 9783527608959. DOI: 10.1002/3527608958.ch27.

[32] Bose. "Plancks Gesetz und Lichtquantenhypothese". In: *Zeitschrift für Physik* 26.1 (1924), pp. 178–181. ISSN: 0044-3328. DOI: 10.1007/BF01327326.

[33] Cheng Chin, Rudolf Grimm, Paul Julienne, and Eite Tiesinga. "Feshbach resonances in ultracold gases". In: *Rev. Mod. Phys.* 82 (2 2010), pp. 1225–1286. DOI: 10.1103/RevModPhys.82.1225.

[34] P. O. Fedichev, Yu. Kagan, G. V. Shlyapnikov, and J. T. M. Walraven. "Influence of Nearly Resonant Light on the Scattering Length in Low-Temperature Atomic Gases". In: *Phys. Rev. Lett.* 77 (14 1996), pp. 2913–2916. DOI: 10.1103/PhysRevLett.77.2913.

[35] M. Theis, G. Thalhammer, K. Winkler, M. Hellwig, G. Ruff, R. Grimm, and J. Hecker Denschlag. "Tuning the Scattering Length with an Optically Induced Feshbach Resonance". In: *Phys. Rev. Lett.* 93 (12 2004), p. 123001. DOI: 10.1103/PhysRevLett.93.123001.

[36] S. Blatt, T. L. Nicholson, B. J. Bloom, J. R. Williams, J. W. Thomsen, P. S. Julienne, and J. Ye. "Measurement of Optical Feshbach Resonances in an Ideal Gas". In: *Phys. Rev. Lett.* 107 (7 2011), p. 073202. DOI: 10.1103/PhysRevLett.107.073202.

[37] Rekishu Yamazaki, Shintaro Taie, Seiji Sugawa, and Yoshiro Takahashi. "Submicron Spatial Modulation of an Interatomic Interaction in a Bose-Einstein Condensate". In: *Phys. Rev. Lett.* 105 (5 2010), p. 050405. DOI: 10.1103/PhysRevLett.105.050405.

[38] S. Yi and L. You. “Trapped atomic condensates with anisotropic interactions”. In: *Phys. Rev. A* 61 (4 2000), p. 041604. DOI: 10.1103/PhysRevA.61.041604.

[39] S. Yi and L. You. “Trapped condensates of atoms with dipole interactions”. In: *Phys. Rev. A* 63 (5 2001), p. 053607. DOI: 10.1103/PhysRevA.63.053607.

[40] N Bogoliubov. “On the theory of superfluidity”. In: *J. Phys* 11.1 (1947), p. 23.

[41] E. P. Gross. “Structure of a quantized vortex in boson systems”. In: *Il Nuovo Cimento (1955-1965)* 20.3 (1961), pp. 454–477. ISSN: 1827-6121. DOI: 10.1007/BF02731494.

[42] Lev P Pitaevskii. “Vortex lines in an imperfect Bose gas”. In: *Sov. Phys. JETP* 13.2 (1961), pp. 451–454.

[43] M Baranov, Ł Dobrek, K Góral, L Santos, and M Lewenstein. “Ultracold Dipolar Gases – a Challenge for Experiments and Theory”. In: *Physica Scripta* 2002.T102 (2002), p. 74. DOI: 10.1238/Physica.Topical.102a00074.

[44] Shai Ronen, Daniele C. E. Bortolotti, D. Blume, and John L. Bohn. “Dipolar Bose-Einstein condensates with dipole-dependent scattering length”. In: *Phys. Rev. A* 74 (3 2006), p. 033611. DOI: 10.1103/PhysRevA.74.033611.

[45] D. C. E. Bortolotti, S. Ronen, J. L. Bohn, and D. Blume. “Scattering Length Instability in Dipolar Bose-Einstein Condensates”. In: *Phys. Rev. Lett.* 97 (16 2006), p. 160402. DOI: 10.1103/PhysRevLett.97.160402.

[46] D. S. Petrov, G. V. Shlyapnikov, and J. T. M. Walraven. “Regimes of Quantum Degeneracy in Trapped 1D Gases”. In: *Phys. Rev. Lett.* 85 (18 2000), pp. 3745–3749. DOI: 10.1103/PhysRevLett.85.3745.

[47] D. S. Petrov, M. Holzmann, and G. V. Shlyapnikov. “Bose-Einstein Condensation in Quasi-2D Trapped Gases”. In: *Phys. Rev. Lett.* 84 (12 2000), pp. 2551–2555. DOI: 10.1103/PhysRevLett.84.2551.

[48] D.S. Petrov, D.M. Gangardt, and G.V. Shlyapnikov. “Low-dimensional trapped gases”. In: *J. Phys. IV France* 116 (2004), pp. 5–44. DOI: 10.1051/jp4:2004116001.

[49] Markus Greiner, Immanuel Bloch, Olaf Mandel, Theodor W. Hänsch, and Tilman Esslinger. “Exploring Phase Coherence in a 2D Lattice of Bose-Einstein Condensates”. In: *Phys. Rev. Lett.* 87 (16 2001), p. 160405. DOI: 10.1103/PhysRevLett.87.160405.

[50] A. Görlitz et al. “Realization of Bose-Einstein Condensates in Lower Dimensions”. In: *Phys. Rev. Lett.* 87 (13 2001), p. 130402. DOI: 10.1103/PhysRevLett.87.130402.

[51] F. Schreck, L. Khaykovich, K. L. Corwin, G. Ferrari, T. Bourdel, J. Cubizolles, and C. Salomon. “Quasipure Bose-Einstein Condensate Immersed in a Fermi Sea”. In: *Phys. Rev. Lett.* 87 (8 2001), p. 080403. DOI: 10.1103/PhysRevLett.87.080403.

[52] Elliott H. Lieb and Werner Liniger. “Exact Analysis of an Interacting Bose Gas. I. The General Solution and the Ground State”. In: *Phys. Rev.* 130 (4 1963), pp. 1605–1616. DOI: 10.1103/PhysRev.130.1605.

[53] Elliott H. Lieb. “Exact Analysis of an Interacting Bose Gas. II. The Excitation Spectrum”. In: *Phys. Rev.* 130 (4 1963), pp. 1616–1624. DOI: 10.1103/PhysRev.130.1616.

[54] Toshiya Kinoshita, Trevor Wenger, and David S. Weiss. “A quantum Newton’s cradle”. In: *Nature* 440.7086 (2006), pp. 900–903. ISSN: 1476-4687. DOI: 10.1038/nature04693.

[55] Yijun Tang, Wil Kao, Kuan-Yu Li, Sangwon Seo, Krishnanand Mallayya, Marcos Rigol, Sarang Gopalakrishnan, and Benjamin L. Lev. “Thermalization near Integrability in a Dipolar Quantum Newton’s Cradle”. In: *Phys. Rev. X* 8 (2 2018), p. 021030. DOI: 10.1103/PhysRevX.8.021030.

[56] L. Landau. “Theory of the Superfluidity of Helium II”. In: *Phys. Rev.* 60 (4 1941), pp. 356–358. DOI: 10.1103/PhysRev.60.356.

[57] D. G. Henshaw and A. D. B. Woods. “Modes of Atomic Motions in Liquid Helium by Inelastic Scattering of Neutrons”. In: *Phys. Rev.* 121 (5 1961), pp. 1266–1274. DOI: 10.1103/PhysRev.121.1266.

[58] L. Santos, G. V. Shlyapnikov, and M. Lewenstein. “Roton-Maxon Spectrum and Stability of Trapped Dipolar Bose-Einstein Condensates”. In: *Phys. Rev. Lett.* 90 (25 2003), p. 250403. DOI: 10.1103/PhysRevLett.90.250403.

[59] D. Petter, G. Natale, R. M. W. van Bijnen, A. Patscheider, M. J. Mark, L. Chomaz, and F. Ferlaino. “Probing the Roton Excitation Spectrum of a Stable Dipolar Bose Gas”. In: *Phys. Rev. Lett.* 122 (18 2019), p. 183401. DOI: 10.1103/PhysRevLett.122.183401.

[60] L. Chomaz, R. M. W. van Bijnen, D. Petter, G. Faraoni, S. Baier, J. H. Becher, M. J. Mark, F. Wächtler, L. Santos, and F. Ferlaino. “Observation of roton mode population in a dipolar quantum gas”. In: *Nature Physics* 14.5 (2018), pp. 442–446. ISSN: 1745-2481. DOI: 10.1038/s41567-018-0054-7.

[61] P. B. Blakie, R. J. Ballagh, and C. W. Gardiner. “Theory of coherent Bragg spectroscopy of a trapped Bose-Einstein condensate”. In: *Phys. Rev. A* 65 (3 2002), p. 033602. DOI: 10.1103/PhysRevA.65.033602.

[62] P. B. Blakie, D. Baillie, and R. N. Bisset. “Roton spectroscopy in a harmonically trapped dipolar Bose-Einstein condensate”. In: *Phys. Rev. A* 86 (2 2012), p. 021604. DOI: 10.1103/PhysRevA.86.021604.

[63] R. N. Bisset and P. B. Blakie. “Fingerprinting Rotons in a Dipolar Condensate: Super-Poissonian Peak in the Atom-Number Fluctuations”. In: *Phys. Rev. Lett.* 110 (26 2013), p. 265302. DOI: 10.1103/PhysRevLett.110.265302.

[64] J. Hertkorn et al. “Density Fluctuations across the Superfluid-Supersolid Phase Transition in a Dipolar Quantum Gas”. In: *Phys. Rev. X* 11 (1 2021), p. 011037. DOI: 10.1103/PhysRevX.11.011037.

[65] Kestutis Staliunas, Stefano Longhi, and Germán J. de Valcárcel. “Faraday Patterns in Bose-Einstein Condensates”. In: *Phys. Rev. Lett.* 89 (21 2002), p. 210406. DOI: 10.1103/PhysRevLett.89.210406.

[66] K. Kwon, K. Mukherjee, S. J. Huh, K. Kim, S. I. Mistakidis, D. K. Maity, P. G. Kevrekidis, S. Majumder, P. Schmelcher, and J.-y. Choi. “Spontaneous Formation of Star-Shaped Surface Patterns in a Driven Bose-Einstein Condensate”. In: *Phys. Rev. Lett.* 127 (11 2021), p. 113001. DOI: 10.1103/PhysRevLett.127.113001.

[67] Chen-Xi Zhu, Wei Yi, Guang-Can Guo, and Zheng-Wei Zhou. “Parametric resonance of a Bose-Einstein condensate in a ring trap with periodically driven interactions”. In: *Phys. Rev. A* 99 (2 2019), p. 023619. DOI: 10.1103/PhysRevA.99.023619.

[68] P. Engels, C. Atherton, and M. A. Hoefer. “Observation of Faraday Waves in a Bose-Einstein Condensate”. In: *Phys. Rev. Lett.* 98 (9 2007), p. 095301. DOI: 10.1103/PhysRevLett.98.095301.

[69] Alexandru I. Nicolin, R. Carretero-González, and P. G. Kevrekidis. “Faraday waves in Bose-Einstein condensates”. In: *Phys. Rev. A* 76 (6 2007), p. 063609. DOI: 10.1103/PhysRevA.76.063609.

[70] Antun Bala ž, Remus Paun, Alexandru I. Nicolin, Sudharsan Balasubramanian, and Radha Ramaswamy. “Faraday waves in collisionally inhomogeneous Bose-Einstein condensates”. In: *Phys. Rev. A* 89 (2 2014), p. 023609. DOI: 10.1103/PhysRevA.89.023609.

[71] R. Nath and L. Santos. “Faraday patterns in two-dimensional dipolar Bose-Einstein condensates”. In: *Phys. Rev. A* 81 (3 2010), p. 033626. DOI: 10.1103/PhysRevA.81.033626.

[72] B. Kh. Turmanov, B. B. Baizakov, and F. Kh. Abdullaev. “Generation of density waves in dipolar quantum gases by time-periodic modulation of atomic interactions”. In: *Phys. Rev. A* 101 (5 2020), p. 053616. DOI: 10.1103/PhysRevA.101.053616.

[73] Dušan Vudragović and Antun Balaž. “Faraday and Resonant Waves in Dipolar Cigar-Shaped Bose-Einstein Condensates”. In: *Symmetry* 11.9 (2019). ISSN: 2073-8994. DOI: 10.3390/sym11091090.

[74] D. K. Maity, K. Mukherjee, S. I. Mistakidis, S. Das, P. G. Kevrekidis, S. Majumder, and P. Schmelcher. “Parametrically excited star-shaped patterns at the interface of binary Bose-Einstein condensates”. In: *Phys. Rev. A* 102 (3 2020), p. 033320. DOI: 10.1103/PhysRevA.102.033320.

[75] Antun Bala ž and Alexandru I. Nicolin. “Faraday waves in binary nonmiscible Bose-Einstein condensates”. In: *Phys. Rev. A* 85 (2 2012), p. 023613. DOI: 10.1103/PhysRevA.85.023613.

[76] Huan Zhang, Sheng Liu, and Yong-Sheng Zhang. “Faraday patterns in spin-orbit-coupled Bose-Einstein condensates”. In: *Phys. Rev. A* 105 (6 2022), p. 063319. DOI: 10.1103/PhysRevA.105.063319.

[77] Michał Matuszewski. “Rotonlike Instability and Pattern Formation in Spinor Bose-Einstein Condensates”. In: *Phys. Rev. Lett.* 105 (2 2010), p. 020405. DOI: 10.1103/PhysRevLett.105.020405.

[78] Sandra M. Jose, Komal Sah, and Rejish Nath. “Patterns, spin-spin correlations, and competing instabilities in driven quasi-two-dimensional spin-1 Bose-Einstein condensates”. In: *Phys. Rev. A* 108 (2 2023), p. 023308. DOI: 10.1103/PhysRevA.108.023308.

[79] D. Edler, C. Mishra, F. Wächtler, R. Nath, S. Sinha, and L. Santos. “Quantum Fluctuations in Quasi-One-Dimensional Dipolar Bose-Einstein Condensates”. In: *Phys. Rev. Lett.* 119 (5 2017), p. 050403. DOI: 10.1103/PhysRevLett.119.050403.

[80] A. Pricoupenko and D. S. Petrov. “Higher-order effective interactions for bosons near a two-body zero crossing”. In: *Phys. Rev. A* 103 (3 2021), p. 033326. DOI: 10.1103/PhysRevA.103.033326.

[81] Chen-Lung Hung, Xibo Zhang, Li-Chung Ha, Shih-Kuang Tung, Nathan Gemelke, and Cheng Chin. “Extracting density–density correlations from in situ images of atomic quantum gases”. In: *New Journal of Physics* 13.7 (2011), p. 075019. DOI: 10.1088/1367-2630/13/7/075019.

[82] Holger Kadau, Matthias Schmitt, Matthias Wenzel, Clarissa Wink, Thomas Maier, Igor Ferrier-Barbut, and Tilman Pfau. "Observing the Rosensweig instability of a quantum ferrofluid". In: *Nature* 530.7589 (2016), pp. 194–197. ISSN: 1476-4687. DOI: 10.1038/nature16485.